

# Theoretical Priors and the Dark Energy Equation of State

Ido Ben-Dayan<sup>1</sup> and Utkarsh Kumar<sup>1</sup>

<sup>1</sup>*Physics Department, Ariel University, Ariel 40700, Israel*

(Dated: October 24, 2023)

We revisit the theoretical priors used for inferring Dark Energy (DE) parameters. Any DE model must have some form of a tracker mechanism such that it behaved as matter or radiation in the past. Otherwise, the model is fine-tuned. We construct a model-independent parametrization that takes this prior into account and allows for a relatively sudden transition between radiation/matter to DE behavior. We match the parametrization with current data, and deduce that the adiabatic and effective sound speeds of DE play an important role in inferring the cosmological parameters. We find that there is a preferred transition redshift of  $1 + z \simeq 29 - 30$ , and some reduction in the Hubble and Large Scale Structure tensions.

## I. INTRODUCTION

The standard  $\Lambda$  cold dark matter ( $\Lambda$ CDM), also known as the Concordance Model, is a well-established cosmological model supported by data from numerous observations. The  $\Lambda$ CDM parameters have been constrained using the cosmic microwave background (CMB) measurements [1–3], supernovae type Ia [4], weak lensing [5–8], and galaxy clustering measurements [9–17] with about a percent accuracy. Despite its remarkable success, the validity of the Concordance Model is under investigation, as accumulation of data results in tensions between various measurements. The last parameter that was added to the Concordance Model, was the cosmological constant,  $\Lambda$ . The presence of a dominant positive cosmological constant explains the present acceleration of the Universe. Except its relative energy density,  $\Omega_\Lambda$ , it should manifest itself in observations by an equation of state (eos)  $w = -1$ . This minimal  $\Lambda$ CDM model is still an excellent fit to data with  $\Omega_\Lambda \simeq 0.70$ . Considering a constant eos without imposing  $w = -1$ , the data further constrains the eos to be  $-1.14 < w < -0.94$  [2, 18]<sup>1</sup>. A true constant, based on zero modes quantum fluctuations of the fields present in

---

<sup>1</sup> This model is usually dubbed  $w$ CDM.

Nature, is expected to be many orders of magnitude above the observed value and there have been many attempts to reconcile the measurement with the theoretical expectation [19–29]. This unappealing mismatch between theory and observations prompted the idea that the present acceleration is due to an evolving (usually scalar) field, dubbed Dark Energy (DE) [30, 31]. Generically, this scalar field is not solving the so-called "old" cosmological constant problem (of the expected zero modes contribution to the energy density of the Universe). Nevertheless, assuming this question is somehow settled, the DE gives predictions for the present acceleration of the Universe. If DE is realized in Nature then generically the eos is time/redshift dependent  $w(z)$ . Furthermore, the DE fluid/field will have fluctuations that will affect the growth of structure [32–35], thus providing a testable framework. Focusing on the eos, there are many possible parametrizations [36–44], perhaps most notably the CPL parametrization [36, 37]

$$w(z) \simeq w_0 + w_1 \frac{z}{1+z}, \quad (1)$$

which is not valid at all redshifts. Combining Planck with BAO and Supernovae data then gives  $w_0 = -0.957 \pm 0.080$ ,  $w_1 = -0.29_{-0.26}^{+0.32}$  [2]. Since DE is evolving with time, another tuning problem arises - why should its energy density and eos be such that it behaves nearly as a cosmological constant today [45–47]? To avoid this coincidence, DE models are generically endowed with a tracker mechanism. The DE tracks the radiation or matter throughout the evolution of the Universe, until it decouples and acts as DE today [48, 49]. We would like to include this theoretical prior into the parameter estimation analysis.

In addition to theoretical difficulties, the values of some cosmological parameters inferred from different cosmological and astrophysical data are in tension with the Planck 2018 parameters for  $\Lambda$ CDM [2]. Perhaps the most intriguing tensions are the Hubble  $H_0$  and Large Scale Structure  $S_8$  tension. The Hubble tension arises from the discrepancy in the measurement of the present value of the Hubble parameter between the model-dependent and model-independent probes. Currently, there is a  $\sim 5\sigma$  discrepancy between the SH0ES (model-independent) [50–63] and Planck 2018 CMB (model-dependent) measurements [2]. However, in addition to the aforementioned measurements, the discrepancy in present day expansion rate persists when considering other experiments and data sets, see [64] and references therein.

$S_8 = \sigma_8 \sqrt{\Omega_m/0.3}$  is a parameter measuring linear fluctuations, where  $\sigma_8$  is the amplitude of linear fluctuations smoothed over  $8\text{Mpc } h^{-1}$ , and  $\Omega_m$  is the relative matter density today.

In inferring  $S_8$  there again seems to be a  $2 - 3\sigma$  discrepancy between Planck and Weak Lensing experiments, e.g. [2, 65–73]. Various solutions have been proposed to solve both tensions individually [31, 53, 54, 58, 64–71, 73–140, 140, 141, 141, 142, 142, 143, 143, 144, 144, 145, 145, 146, 146, 147]. Some solutions resolving the Hubble tension seem to worsen the LSS tension or vice-versa [35, 90, 124–126, 148]. A theory that addresses both of these conflicts at once would undoubtedly be appealing, so in this study we make a point of attempting to handle the  $S_8$  and  $H_0$  tensions concurrently [149–151].

Recently, we have suggested an emerging DE model. In this model the DE is not a fundamental scalar field, but rather a thermodynamical collective behavior [149–151]. This approach solves the fine tuning and initial conditions problems, is free of the swampland conjectures [152–159] and does not modify gravity. The model has a built in tracker mechanism since it asymptotes to  $w = -1$  at future infinity and to  $w = 1/3$  in the past - i.e. the fluid behaves as radiation in the past and transitions to DE behavior at some redshift. Our recent analysis shows that the model is restoring cosmological concordance and alleviating both the Hubble tension and the  $S_8$  tension, performing significantly better than  $\Lambda$ CDM [149]. Motivated by this success, we want to investigate whether this behavior is more generic.

Since any valid DE model has  $w(z = 0) \simeq -1$  and any model with a tracker mechanism  $w(z \gg 1) = 1/3$  or  $0$ , we can implement this understanding into our parametrization. We can then test the novel parametrization and its effect on existing tensions such as the Hubble or  $S_8$  tensions. We develop a phenomenological approach where at the most economical level is:

$$w_{DE}(a) = -1 + \frac{w_a}{1 + (a/a_t)^n}, \quad (2)$$

where  $n$  is some integer,  $a_t$  is a transition scale factor around which  $w_{DE}$  transitions from  $w_{DE} \simeq -1$  to  $w_{DE} \simeq -1 + w_a$ . To demonstrate our approach, we shall consider the possibility  $w_a = 4/3$ , such that the DE behaves as radiation at early times. Thus, the parameter that has to be inferred from measurements is neither  $w_0$  nor  $w_a$ , but rather the transition redshift/scale factor  $a_t$ . In this minimal approach  $c_s^2$  is determined. So we are fitting less parameters than the usual CPL parametrization. We then extend our model to include  $c_s$  and later also  $n$  as free parameters. We calculate the background and perturbations evolution and match to existing data. We then perform a likelihood analysis of our model combining various data sets. We find some modest reduction in the Hubble and  $S_8$  tension

and some reduction in  $\Delta\chi^2 \sim -2 - -3$  compared to  $\Lambda$ CDM. The more interesting result is that we find the transition redshift to be highly constrained,  $z_t = 29 - 30$ , providing a definite interval for exploration.

The paper is organized as follows. We first describe the details of background and perturbation evaluation of our proposed phenomenological fluid parametrization in section II. Next, in section III we discuss different data sets and methods used to analyze our proposed parametrization. This section includes the nomenclature of different models used, combinations of datasets and measures the assess the  $H_0$  and  $S_8$  tensions. Sections IV deals with the results and finally we conclude in section V

## II. PHENOMENOLOGICAL FLUID DARK ENERGY

We propose a scenario consisting of the standard cosmological model with cold dark matter (CDM) and DE using a phenomenological fluid with several critical key features which differ from the cosmological constant (CC). In this section will discuss the model, its background, and perturbative dynamics. Using our approach, we also illustrate the implications on cosmological tensions, such as Hubble ( $H_0$ ) and Large Scale Structure  $S_8$ .

### A. Theory

Our proposed scenario mimics  $\Lambda$ , which is used to account for Dark Energy in late times and transits to radiation at early times. The model is specified by a time-varying equation of state for such phenomenological fluid.

***Conditions of DE model*** We start our discussion by pointing out the conditions for a successful Dark Energy Model as

- The Dark Energy model should be able to explain cosmic coincidence and the hierarchy problem of DE, e.g.,  $\Lambda$ .
- There should be an era of dust domination, which is essential for the structure of the Universe.
- The equation of state of DE component today, defined as  $w_{DE} = \frac{p_{DE}}{\rho_{DE}}$  where  $\rho_{DE}$  and  $p_{DE}$  being the energy density and pressure of the DE fluid respectively, must lie within  $-1.14 < w_{DE} < -0.94$  [2, 18].

- The evolution of DE fluid and hence the whole background and perturbative evolution of the Universe should be free from instability. Thus, there should be no gradient instability and the sound speed of DE fluid should be subluminal, i.e.,  $0 < c_{DE,a}^2 < 1$ . Here  $c_{DE,a}^2 = \frac{\dot{\rho}_{DE}}{\rho_{DE}}$  is the squared sound speed of DE fluid.

**Background** The time-varying eos of a phenomenological fluid ( $w_{DE}$ ) is governed by the following form

$$w_{DE}(a) = -1 + \frac{w_a}{1 + (a/a_t)^n}, \quad (3)$$

where we normalize the scale factor  $a$  to be unity today. Equation (3) asymptotes to  $w_{DE}(a) = -1 + w_a$  and  $w_{DE}(a) = -1$  at early and late times respectively.  $w_a$  tunes the desired eos of state of the Dark Energy fluid at early times, and  $a_t$  is the "transition scale factor" or redshift at which the fluid approximately crosses  $w_{DE} = 0$ . The parameter  $n$  controls the sharpness of this transition. Using the equation (3), it is straightforward to derive the energy density of the fluid as

$$\rho_{DE}(a) = \rho_{DE,0} a^{-3w_a} \left( \frac{1 + (a/a_t)^n}{1 + (1/a_t)^n} \right)^{3w_a/n}. \quad (4)$$

Equations (3) and (4) give us a full picture of the background for our Dark Energy model as a phenomenological fluid with up to 3 parameter extension to  $\Lambda$ CDM.

Our proposal for Dark Energy using **P**henomenological **F**luid **D**ark **E**nergy (PFDE) has a built-in tracker mechanism that tracks the background throughout evolution. Since we would like the PFDE to track the background evolution of the Universe as a whole, we require that the eos of phenomenological fluid will lie within  $\in [0, 1/3]$  at early times, which constrains  $w_a$  as

$$w_{DE}^{Early} \approx -1 + w_a \in [0, 1/3] \Rightarrow w_a \in [1, 4/3] \quad (5)$$

We think the new parametrization has several advantages over existing ones: First, it captures the essence of DE with  $w \simeq -1$ . Second, it captures the tracker behavior of  $w = 1/3$  at large redshift. Third, there is a single free parameter - the transition redshift or scale factor  $a_t$ . Thus, in terms of the number of cosmological parameters it is equivalent to  $w$ CDM with fixed  $w$ . Later, when we allow for an arbitrary  $c_s^2$ , we have the same number of parameters as the CPL one, but with different theoretical input.

Let us demonstrate the behavior of the model. First, we present examples of the effect of the steepness of transition and transition redshift on the DE eos  $w_{DE}$  in Figure 1. It is clear from the plots that  $w_{DE}$  transits from  $1/3$  to  $-1$ , with different transition steepness (from varying  $n$ ) and at different transition redshifts (varying  $a_t$ ), at early and late times.

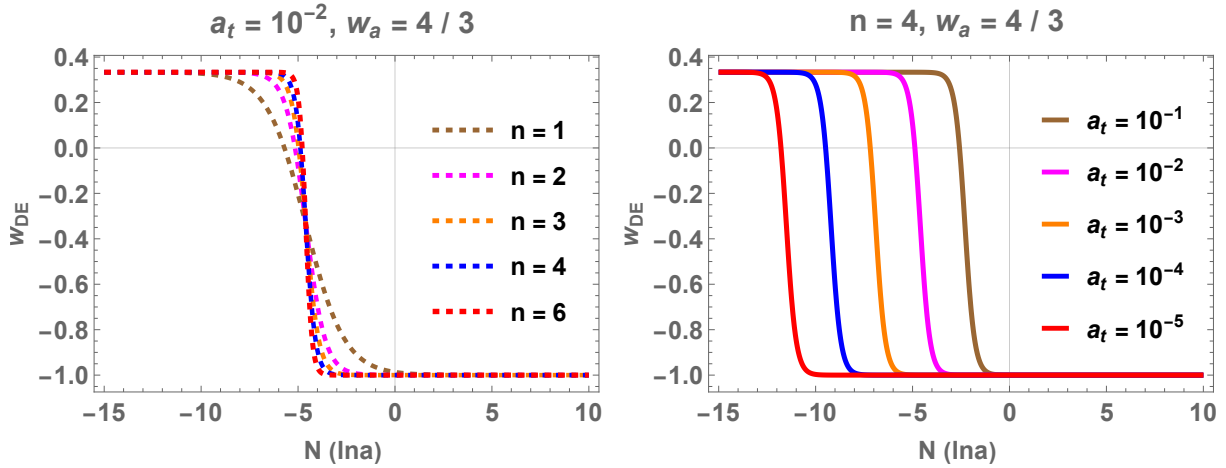


FIG. 1: Evolution of Dark Energy equation of state  $w_{DE}$  as a function of e-folds,  $N = \ln a$ , for different values of  $n$  and  $a_t$  while fixing other parameters in left and right panels respectively.

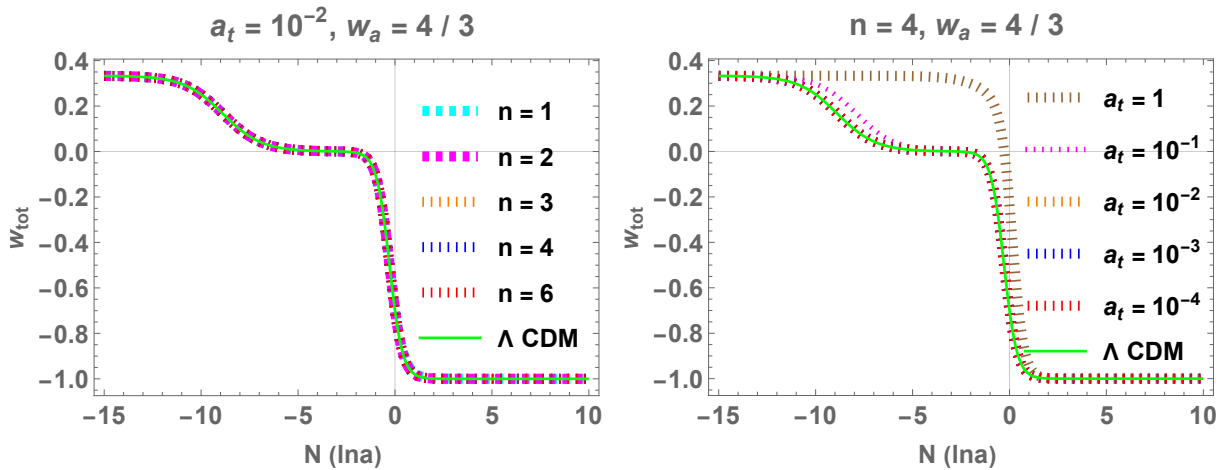


FIG. 2: Evolution of total equation of state ( $w_{tot}$ ) as a function of e-folds,  $N = \ln a$ , for different values of  $n$  and  $a_t$  while fixing other parameters in left and right panels respectively.

Next, we discuss the evolution of the effective eos of the Universe,  $w_{tot}$ . There is almost no difference from the standard  $\Lambda$ CDM for different values  $n$  while there is a strong dependence of  $a_t$  on  $w_{tot}$  as shown in the left and right panel of fig (2). It is evident from the right panel

of fig (2), that as we increase the value of  $a_t$ , DE+radiation dominate over the matter sector and we see no era of dust domination which is crucial for structure formation. Thus, we limit  $a_t \leq 0.1$ . Finally, we compare the expansion rate of PFDE model and  $\Lambda$ CDM using the best fit model parameters inferred from the combination of all data sets. To appreciate the increase in expansion rate in our model, we present our results normalized with respect to the expansion rate of  $\Lambda$ CDM. In the left and right panel of Fig. 3, we show the dependence of  $H_{PFDE}/H_\Lambda$  on  $n$  and  $a_t$  respectively. In all cases the inferred Hubble parameter in the PFDE model is larger than the  $\Lambda$ CDM one.

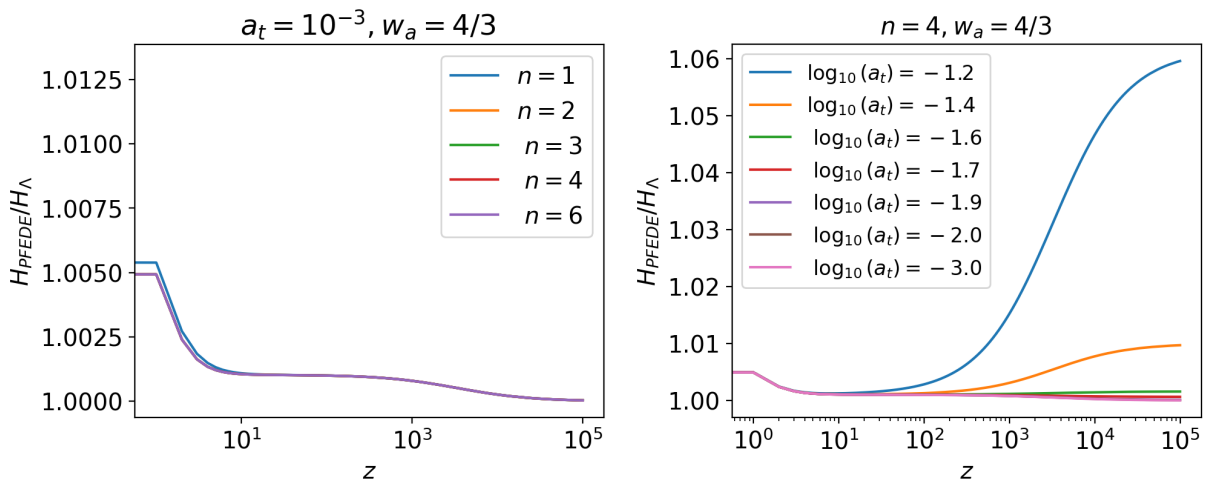


FIG. 3: Comparison of the expansion rate of PFDE model and  $\Lambda$ CDM using their best fit parameters inferred from All data sets. We plot the  $H_{PFDE}/H_\Lambda$  with varying  $n$  and  $a_t$  in the left and right panels respectively.

**Perturbations** The evolution of perturbations depends on the sound horizon of DE. In the FLRW Universe, the sound horizon of DE with effective sound speed  $c_s$  is defined as

$$r_s(\eta) = \int \frac{c_s}{a \mathcal{H}} d\eta, \quad (6)$$

where  $\mathcal{H}(\equiv a'/a)$  is the conformal Hubble constant, and  $'$  denotes derivative with respect to conformal time  $\eta$ . Depending on the properties of the fluid, it will have different clustering effects, and  $c_s$  plays crucial role in the evolution of DE perturbation. If  $c_s$  to close to unity, DE perturbations are suppressed by pressure. As a result DE does not cluster except on scales comparable to the  $r_s$ . In the case of  $c_s \ll 1$ , DE starts clustering as a dark matter component with the consequence of affecting matter perturbations. Finally, a more

general effective speed of sound  $0 \leq c_s^2 \leq 1$ , for example from non-canonical scalar fields or unparticles can result in different forms of clustering.

Any phenomenological fluid is characterized by the energy density  $\rho_{DE}$ , pressure  $p_{DE}$ , momentum density, and anisotropic stress  $\sigma_{DE}$ . The pressure  $\delta p_{DE}$  and energy density perturbations  $\delta \rho_{DE}$  are related by the effective sound speed which is gauge dependent quantity  $c_s^2 = \frac{\delta p_{DE}}{\delta \rho_{DE}}$ . For canonical scalar field models, it is automatically set to unity. To avoid such gauge ambiguities, we consider the gauge invariant formulation of pressure perturbation Fourier space allowing for a general effective sound speed discussed in [160].

$$\delta p_{DE} = c_s^2 \delta \rho_{DE} + 3 \mathcal{H} (c_s^2 - c_a^2) (1 + w_{DE}) \rho_{DE} \theta_{DE} / k^2. \quad (7)$$

Here  $\theta_{DE}$  is the velocity divergence, and  $c_a^2$  is the adiabatic sound speed for our phenomenological fluid, which takes the following form

$$c_a^2 \equiv w_{DE} - \frac{w'_{DE}}{3 \mathcal{H} (1 + w_{DE})} = w_{DE} - \frac{n}{3 w_a} (1 + w_{DE} - w_a), \quad (8)$$

where for  $w_a = 4/3$  we have  $c_a^2 = w_{DE}(1 - \frac{n}{4}) + \frac{n}{12}$ . The adiabatic sound speed and its dependence on the model parameters are depicted in figure 4. Notice that for  $n < 3$  the adiabatic speed of sound tends to negative values, raising the danger of instabilities. We will see that even without addressing this theoretical issue, the data will prefer  $n \geq 3$ .

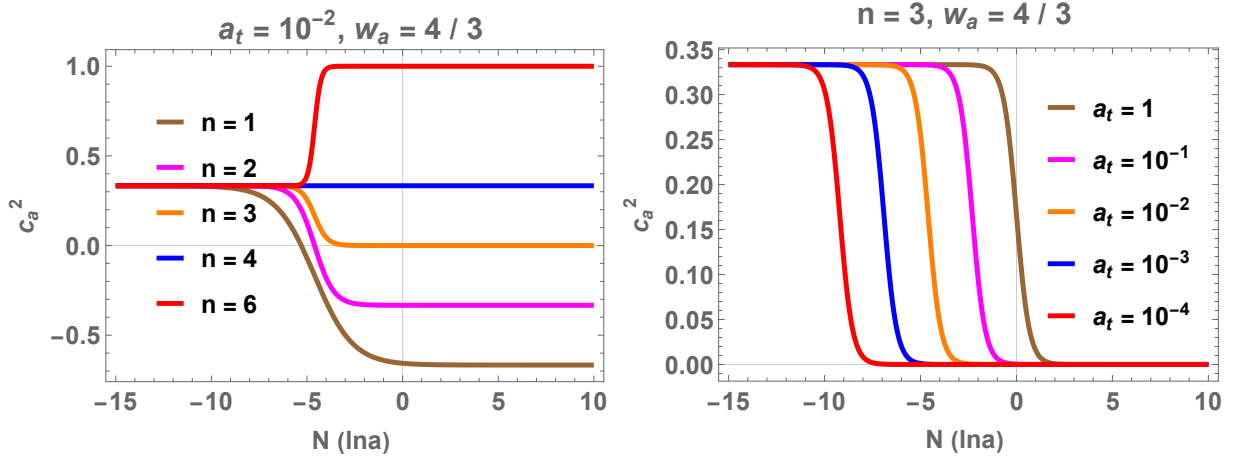


FIG. 4: The evolution of adiabatic sound speed  $c_a^2$  for PFDE model parameters. The left panel shows that adiabatic sound speed becomes negative at the late time for  $n < 3$ . The right panel illustrates the transition of  $c_a^2$  for different values of  $a_t$ .

We write the perturbation equations in synchronous gauge with the following line element:

$$ds^2 = a^2(\eta) [-d\eta^2 + (\eta_{ij} + h_{ij}) dx^i dx^j], \quad (9)$$

where  $h(\equiv h_i^i)$  is the metric perturbation and  $\sigma_{DE}$  is the anisotropic stress [161]. Within the gauge invariant formalism, we express the perturbations as equations of the density contrast  $\delta_{DE}$  and the velocity divergence  $\theta_{DE}$ :

$$\delta'_{DE} = -(1 + w_{DE}) (\theta_{DE} - 3h') - 3\mathcal{H} (c_s^2 - w_{DE}) \delta_{DE}, \quad (10)$$

$$\theta'_{DE} = -\mathcal{H} (1 - 3w_{DE}) \theta_{DE} - \frac{w'_{DE}}{1 + w_{DE}} \theta_{DE} + \frac{c_s^2}{1 + w_{DE}} k^2 \delta_{DE} + k^2 (h - \sigma). \quad (11)$$

It is straightforward to figure out that perturbations of dark energy for a phenomenological fluid offers two extra parameters of the model compared to canonical scalar field, namely, the effective sound speed  $c_s^2$  and the anisotropic shear/stress  $\sigma_{DE}$ . In this work, we shall always consider a perfect fluid, so  $\sigma_{DE} \equiv 0$ . For the effective sound speed  $c_s$  there are various possibilities. The effective sound speed  $c_s$  importance cannot be underestimated as it reveals the microphysics associated to dark energy. For a barotropic fluid it is equivalent to adiabatic sound speed of the fluid,  $c_s \equiv c_a$ . As such no free parameters are introduced. A nice example of such a scenario is the Unparticles Dark Energy (UDE) which offers a possible resolution of Hubble and LSS tension simultaneously [149–151]. Attempting to study different microphysics, we shall consider the following scenarios:

1. Allowing dark energy either to be relativistic  $c_s = 1$  or be non-relativistic  $c_s = 0$ .
2. A perfect fluid, with the  $c_s$  as a free parameter,  $0 \leq c_s \leq 1$ .

### III. DATA SETS AND METHODOLOGY

In our analysis, we use the following publicly available data sets:

- **Planck 2018 CMB** : We utilize the `Planck 2018` likelihood for the CMB data, which consists of the low- $\ell$  TT, low- $\ell$  EE, and high- $\ell$  TTEETE power spectra [3]. We also use the `Planck 2018` lensing likelihood [1], which has an important role in the LSS analysis of the late Universe.
- **Baryon Acoustic Oscillations (BAO) and RSD measurements**: We use the measurements from the SDSS DR7 Main Galaxy Sample (MGS) [9] and 6dF galaxy survey [10] measurements at  $z = 0.15$  and  $z = 0.106$  respectively. In addition to that, we also include BAO and  $f\sigma_8$  measurements (where  $f$  is the linear growth rate) from

BOSS DR12 & 16 at  $z = 0.38, 0.51, 0.68$  [11–14], QSO measurements at  $z = 1.48$  [15, 16] and Ly- $\alpha$  auto-correlation and cross-correlation with QSO at  $z = 2.2334$  [17].

- **Large Scale Structure:**

- **DES:** Dark Energy Survey includes measurements from shear-shear, galaxy-galaxy, and galaxy-shear two-point correlation functions, referred to as "3 $\times$ 2 pt", measured from 26 million source galaxies in four redshifts bins and 650,000 luminous red lens galaxies in five redshifts bins, for the shear and galaxy correlation functions [5]. DES 3  $\times$  2 pt likelihood gives  $S_8 = 0.773^{+0.026}_{-0.020}$  and  $\Omega_m = 0.267^{+0.030}_{-0.017}$  for  $\Lambda$ CDM model. To avoid the computational expenses, we use the Gaussian prior on  $S_8$  which effectively summarize the DES likelihood. We also confirm that using the Gaussian prior and DES likelihood provide a similar constraint.

- **Weak Lensing Measurements:** In addition to the DES measurements, we also use the measurements from KiDS+VIKING-450 and Subaru Hyper Suprime-Cam (HSC) providing constraints on  $S_8$  and  $\Omega_m$ . In this case also we use Gaussian priors to include their effects. We use  $S_8 = 0.737^{+0.040}_{-0.036}$  and  $S_8 = 0.780^{+0.030}_{-0.033}$  for KiDS and HSC measurements respectively.

- **Supernovae Pantheon:** The Pantheon data set is a collection of the absolute magnitude of 1048 supernovae distributed in redshift interval  $0.01 < z < 2.26$  [4]. Many times we will simply refer to this data set as SN.

- **$H_0$  from SHOES:** We use latest local measurement of  $H_0 = 73.04 \pm 1.04$  km/sec/Mpc from the SHOES team [54]. Many times we will simply refer to this data set as  $H_0$ .

We consider several combinations of datasets to assess the parameter constraints of our phenomenological fluid dark energy model. Our aim is to compare the value of  $H_0$  and  $S_8$  inferred considering our model compared to the baseline model  $\Lambda$ CDM. In order to quantify the degree of tension between the different estimates of  $H_0$ , we adopt the following measure to evaluate the improvement of our model compared to  $\Lambda$ CDM. We express the tension in

terms of standard deviations  $\sigma$  for  $H_0$  and  $S_8$  as

$$\# \sigma_{H_0} = \left| \frac{H_0^M - H_0^{\text{SHOES}}}{\sqrt{\sigma_{H_0^M}^2 + \sigma_{H_0^{\text{SHOES}}}^2}} \right|, \quad (12)$$

$$\# \sigma_{S_8} = \left| \frac{S_8^M - S_8^{\text{LSS}}}{\sqrt{\sigma_{S_8^M}^2 + \sigma_{S_8^{\text{LSS}}}^2}} \right|. \quad (13)$$

Here  $x^M$  and  $\sigma_x^M$  are the mean value of parameter  $x$  and its variance in a given model respectively. In the case of two measurements with asymmetric error bars  $X_{\sigma_{X,\text{down}}^{\sigma_{X,\text{up}}}}$ ,  $Y_{\sigma_{Y,\text{down}}^{\sigma_{Y,\text{up}}}}$ , then the tension  $\sigma$  between the two measurements is:

$$\sigma = \begin{cases} \frac{X-Y}{\sqrt{\sigma_{X,\text{down}}^2 + \sigma_{Y,\text{up}}^2}} & \text{if } X > Y \\ \frac{Y-X}{\sqrt{\sigma_{X,\text{up}}^2 + \sigma_{Y,\text{down}}^2}} & \text{if } X \leq Y. \end{cases} \quad (14)$$

We investigate the following combination of datasets:

1. Planck 2018 CMB TTTEEE power spectrum data which is one of the sources of present cosmic tensions. For simplicity, we call this dataset **Planck 2018 CMB**.
2. Combination of Primary Planck 2018 TTTEEE+ lensing data with BAO, SNe, and  $H_0$  priors. This combination will help us understand the impact of adding other non-CMB datasets on the proposed model. We represent this combination as **CBSH**.
3. To understand the large-scale structure ( $S_8$ ) tension, we also consider the full LSS data including DES-Y1, HSC, and KIDS along with Primary Planck 2018 CMB including lensing power spectra, BAO, and SNe datasets with SHOES prior. We denote this combination as **CBSHDK**<sup>2</sup>.
4. Finally, we remove the  $H_0$  while using all other datasets used previously and refer to it as **CBSDK**.

The rationale for the different combinations is to see the effect of each data set on the inferred parameters, and allow for amelioration of the tension. For example, if **CBSH** prefers a lower value of  $S_8$ , closer to the WL values, and with significant  $\Delta\chi^2$  improvement,

---

<sup>2</sup> To analyze all LSS experiments as Gaussian prior on  $S_8$  for each data, there exists a possibility of double counting the LSS information and biasing the results as pointed out in [162]. However, to circumvent this issue, we also perform the MCMC analysis using only a single prior on  $S_8$ . The results are tabulated in Appendices A to C. We thank Gen Ye for pointing out this issue.

then the tension is ameliorated compared to  $\Lambda$ CDM. The models we consider are the  $\Lambda$ CDM as baseline model, and extensions according to various possible PFDE.  $\Lambda$ CDM model has the usual 6 free independent parameters: the Baryon  $\Omega_b h^2$  and Cold Dark Matter  $\Omega_c h^2$  relative energy densities, the Hubble parameter  $H_0$  or the angular scale  $\theta_s$ , the amplitude  $A_s$  and tilt  $n_s$  of the primordial power spectrum and  $\tau_{reio}$  quantifying optical depth to reionization. The PFDE model offers several extra parameters namely : scale factor  $a_t$  at which dark energy eos switches sign,  $n$  the sharpness of transition which in turn affects the adiabatic sound speed  $c_a^2$  as shown in figure 4, and finally the effective sound speed of perturbations  $c_s^2$ . The analysis presented in this paper assumes the models with parameters  $a_t$ ,  $n$  and different values of  $c_s^2$  as

- **Canonical Emergent Dark Energy** : To begin with, we examine the specific case of setting  $c_s^2 = 1$ . These models fall into the category of "Canonical Emergent Dark Energy," which can be realized by employing a canonical scalar field with a suitable potential. By assigning this designation, we distinguish them as a distinct subclass within the broader framework of emergent dark energy models.[163–170]
- **Clustering Emergent Dark Energy** : Next, we assign a value of  $c_s^2$  to zero. Under this circumstance, perturbations in DE exhibit a non-relativistic behavior and cluster akin to dark matter. Numerous investigations have focused on understanding the evolution of these perturbations and the process of structure formation in the context of clustering dark energy.[171–176]
- **Non-Canonical Emergent Dark Energy** : Moreover, we extend the parameter  $c_s^2$  to span the range from 0 to 1. This class of models, known as non-canonical emergent dark energy models, arises from nonstandard scalar field models. In these models, the properties of dark energy are described by considering alternative formulations of scalar fields, leading to emergent behavior that deviates from canonical expectations.[177–181, 181, 182]

We sample the posterior distributions of the parameters describing the aforementioned models by using the Markov Chain Monte Carlo (MCMC) method. The chains are produced using the cosmological MCMC sampler `Cobaya` [183] in conjunction with modified publicly available Einstein-Boltzmann code `CAMB` [184]. The convergence of chains are guaranteed by the Gelman-Rubin parameter [185] with  $R - 1 < 0.03$ . We constrain the standard

cosmological parameters for all cosmologies with uniform priors - the baryon matter density  $\Omega_b h^2 \in [0.005, 0.1]$ , the cold dark matter density  $\Omega_c h^2 \in [0.001, 0.99]$ , the amplitude of primordial curvature spectrum  $\ln(10^{10} A_s) \in [1.6, 3.9]$  evaluated at suitable pivot scale,  $k = 0.05 \text{ Mpc}^{-1}$  along with its tilt  $n_s \in [0.8, 1.2]$ , the reionization optical depth  $\tau_{reio} \in [0.01, 0.8]$  and the present value of Hubble parameter  $H_0 \in [20, 100]$ . We use the standard three neutrino description with one massive with mass,  $m_\nu = 0.06 \text{ eV}$ , and two massless neutrinos. The posterior distributions are in the Supplementary Material. We work with uniform prior for  $a_t$ ,  $n$  and  $c_s^2$  with prior edges given by  $[0.01, 0.1]$ ,  $[1, 6]$  and  $[0, 1]$  respectively.

#### IV. RESULTS

In the following, we discuss the results obtained using the methods and datasets described in the previous section. This section covers the impact of emergent dark energy cosmologies on  $H_0$  and  $S_8$  tensions. We present the 68 % CL parameter inferences for concordance  $\Lambda$ CDM model in Table I. We will compare the results of different models to the  $\Lambda$ CDM parameter constraints.

**The mean  $\pm 1\sigma$  constraints for  $\Lambda$ CDM model**

Parameter	Planck 2018 CMB	CBSH	CBSHDK	CBSDK
$H_0$	$67.30 \pm 0.65$	$68.09^{+0.63}_{-0.41}$	$68.13^{+0.86}_{-0.32}$	$68.16^{+0.37}_{-0.32}$
$\sigma_8$	$0.8117 \pm 0.0079$	$0.8102 \pm 0.0063$	$0.8055 \pm 0.0058$	$0.8056 \pm 0.0060$
$S_8$	$0.833 \pm 0.017$	$0.818^{+0.010}_{-0.015}$	$0.8119^{+0.0082}_{-0.017}$	$0.8114 \pm 0.0094$
$\Omega_m$	$0.3162 \pm 0.0089$	$0.3056^{+0.0051}_{-0.0083}$	$0.3048^{+0.0039}_{-0.011}$	$0.3043^{+0.0040}_{-0.0048}$
$\#\sigma_{H_0}$	4.68	4.07	3.63	4.42
$\#\sigma_{S_8}$	2.28	1.89	1.72	1.81
Total $\chi^2$	2764.17	3854.028	3859.8118	3846.0773
$\Delta\chi^2$	—	—	—	—

TABLE I: The mean  $\pm 1\sigma$  constraints on the cosmological parameters inferred from the various datasets for  $\Lambda$ CDM model.

### A. Canonical Emergent Dark Energy Cosmology

We begin our exploration by delving into the canonical emergent dark model with  $c_s^2 = 1$ , laying the foundation for our subsequent analysis. In order to deduce the constraints on the model parameters, we employ various combinations of data sets as outlined in section III. The resulting parameter constraints at the 68% confidence level (CL) are presented Table II.

Considering Planck 2018 CMB data, we observe a slight increase in the derived value of  $H_0 = 68.27 \pm 0.75$  for the canonical emergent dark energy models, compared to the value of  $H_0 = 67.30 \pm 0.65$  for  $\Lambda$ CDM. This increase is consistent across other combinations of data sets, resulting in a range of  $H_0$  values spanning from 68.3 to 69.03 km/sec/Mpc in all the considered analyses. Consequently, the discrepancy known as the Hubble tension diminishes to a range of  $\sim 3\sigma$  confidence level.

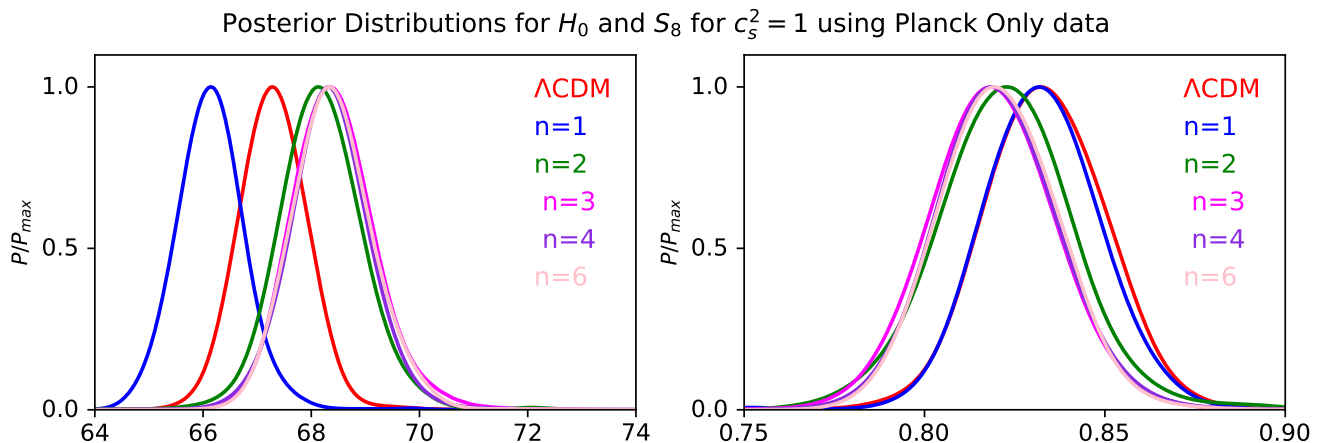


FIG. 5: Normalized posterior distributions for  $H_0$  (in km/sec/Mpc) and  $S_8$  in left and right panels respectively for different choices of  $n$  for Emergent Dark Energy model with  $c_s^2 = 1$  using Primary Planck 2018 CMB data. We also show the constraints for  $\Lambda$ CDM model for comparison.

Moreover, we find a marginal decrease in the inferred values of  $S_8$  within this framework. For instance, when considering only the Planck data, the inferred value of  $S_8$  is  $0.82 \pm 0.016$ , whereas other data sets yield similar values ranging from 0.82 to 0.804. This decrease in  $S_8$  can be attributed to the reduction in matter energy density, which exhibits a decrease of approximately 1%. Moving forward, we shift our focus to the inference of the model parameters  $a_t$  and either  $n$  or  $c_{a_0}^2$ . In order to derive the functional dependence of  $c_{a_0}^2$  on other parameters, one can simply evaluate the eq. 8 at  $z = 0$ . Our analysis reveals that the 68%

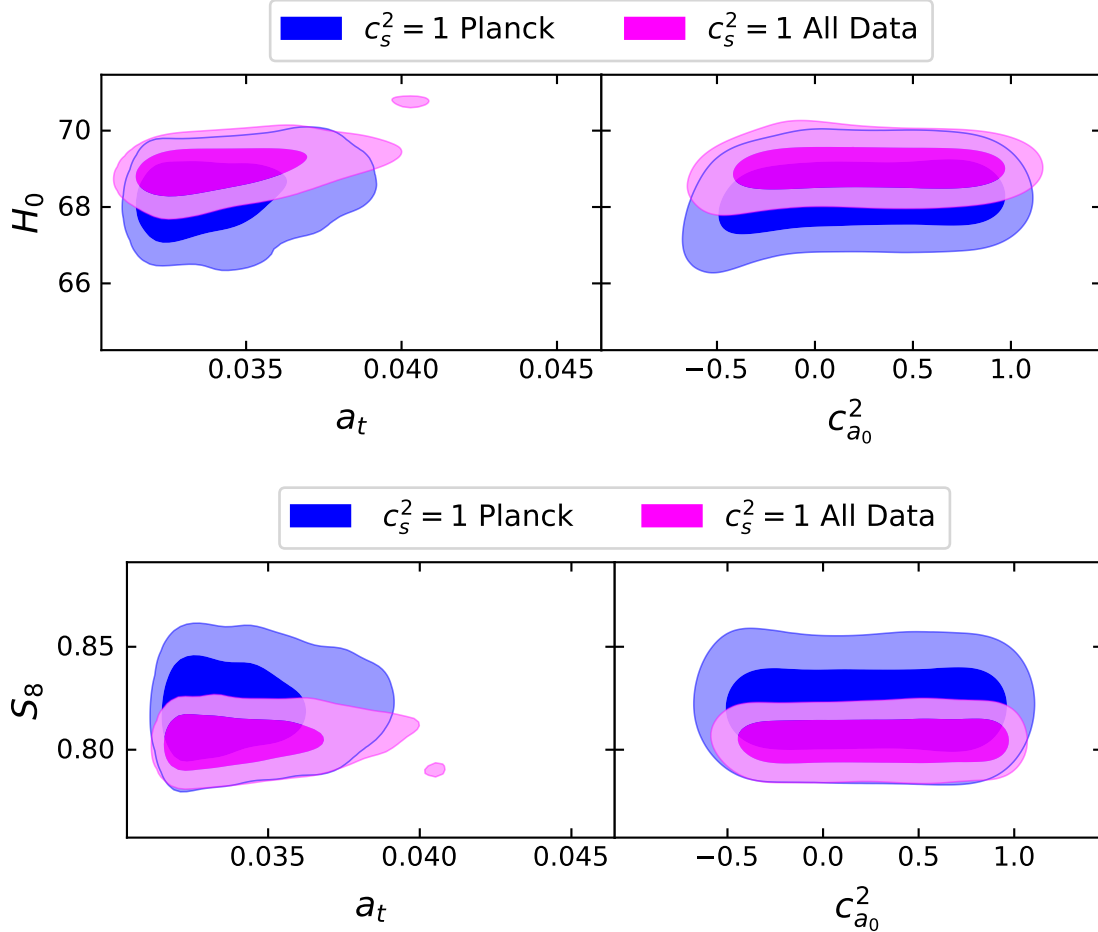


FIG. 6: 2-dimensional marginalized posterior distributions for model parameters  $a_t$  and  $c_{a_0}^2$  (and hence  $n$ ) with  $H_0$  and  $S_8$  in upper and lower panels for canonical emergent dark energy model. The blue and magenta correspond to Primary Planck 2018 CMB data and All Data described in section III

confidence evidence points to  $10^2 a_t = 3.4^{+0.071}_{-0.023}$ . Additionally, we constrain the adiabatic sound speed of dark energy at the present time, denoted as  $c_{a_0}^2$ . The analysis indicates positive adiabatic sound speed with  $c_{a_0}^2 = 0.27^{+0.60}_{-0.36}$  at the 68% CL when considering only the Planck data. Furthermore, we establish a lower bound on the parameter  $n$ , demonstrating that cosmological data favors the canonical emergent dark energy model while excluding the presence of ghost or gradient stability. Our findings indicate  $n > 2.88$ , and Figure (4) confirms that for  $n > 2$ , the adiabatic sound speed lies within the range of  $[0, 1]$ .

We evaluate the goodness-of-fit for various combinations in the canonical emergent dark energy scenario and compare them with  $\Lambda$ CDM. We observe that the fit to the Planck-only

**The mean  $\pm 1\sigma$  constraints for canonical emergent dark energy model ( $c_s^2 = 1$ ) model**

Parameter	Planck 2018 CMB	CBSH	CBSHDK	CBSDK
$H_0$	$68.27 \pm 0.75$	$68.94^{+0.43}_{-0.62}$	$69.03 \pm 0.50$	$68.72 \pm 0.39$
$\sigma_8$	$0.8112 \pm 0.0087$	$0.8134^{+0.0067}_{-0.0078}$	$0.8078 \pm 0.0066$	$0.8070 \pm 0.0062$
$S_8$	$0.820 \pm 0.016$	$0.812 \pm 0.011$	$0.8043 \pm 0.0092$	$0.8081 \pm 0.0087$
$\Omega_m$	$0.3068 \pm 0.0092$	$0.2993^{+0.0067}_{-0.0054}$	$0.2974 \pm 0.0054$	$0.3009 \pm 0.0046$
$10^2 a_t$	$3.400^{+0.071}_{-0.023}$	$3.50^{+0.11}_{-0.32}$	$3.425^{+0.080}_{-0.26}$	$3.368^{+0.056}_{-0.20}$
$c_s^2$	1	1	1	1
$n$	$> 2.86$	$> 3.08$	$> 3.02$	$> 2.88$
$c_{a_0}^2$	$0.23 \pm 0.46$	$0.28 \pm 0.41$	$0.27 \pm 0.43$	$0.24 \pm 0.44$
$\#\sigma_{H_0}$	3.72	3.64	3.47	3.88
$\#\sigma_{S_8}$	1.92	1.80	1.63	1.73
Total $\chi^2$	2766.1977	3852.5094	3857.234	3846.1532
$\Delta\chi^2$	2.0277	-1.5186	-2.5778	0.0759

TABLE II: The mean  $\pm 1\sigma$  constraints on the cosmological parameters inferred from the various datasets for canonical emergent dark energy model ( $c_s^2 = 1$ ) model.

data yields a larger value of  $\Delta\chi^2 = 2.0277$ , indicating a less favorable fit. However, as we combine the Planck data with several other data sets, we witness an improvement reaching approximately  $\Delta\chi^2 = -2.6$  in our analysis.

We also study the impact of different values of  $n$  which in turn means that  $c_{a_0}^2$  is fixed. We fixed the values of  $n$  spanning from 1 to 6. The resulting constraints for different combination are shown in Appendix A (Tables V to IX). The normalized 1-dimensional posterior distributions for  $H_0$  in units of km/sec/Mpc and  $S_8$  for different values of  $n$  in this scenario using the Primary Planck 2018 CMB data in Fig. 5. We notice the increase in inferred value of  $H_0$  and the decrease in the inferred value of  $S_8$  except for  $n = 1$ , which is prone to ghost instability. This trend is present in other data-sets combinations as well.

Finally, we close this subsection by discussing the correlation of model parameters,  $a_t$  and  $c_{a_0}^2$  or  $n$ , with  $H_0$  and  $S_8$  considering the various datasets. Upper and lower panel of Fig. 6 shows the 2-dimensional contours of  $H_0 - (a_t, c_{a_0}^2)$  and  $S_8 - (a_t, c_{a_0}^2)$  respectively. The blue contours are using only Planck data, while the magenta contours take into account all data.

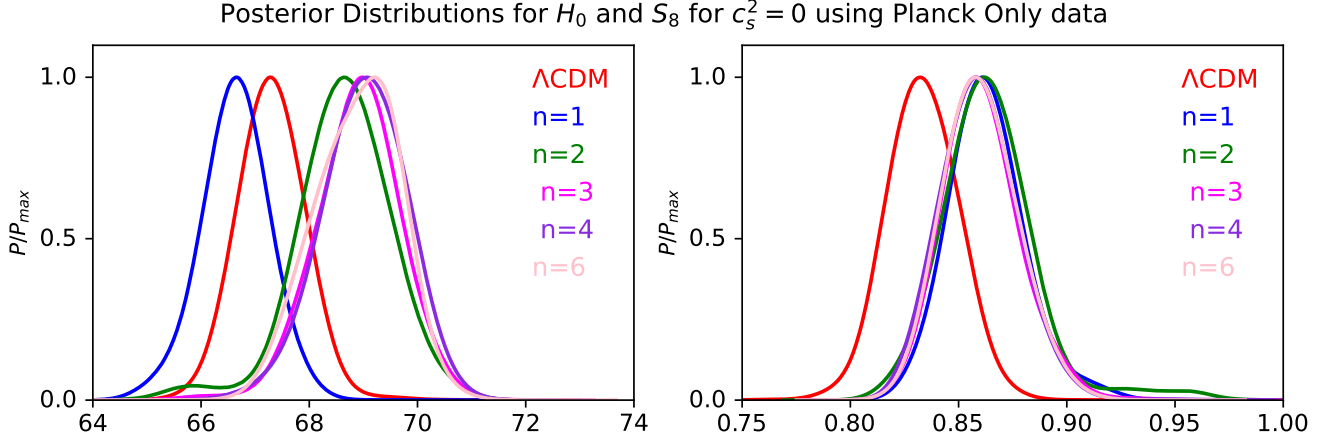


FIG. 7: Normalised posterior distributions for  $H_0$  (in km/sec/Mpc) and  $S_8$  in left and right panels respectively for different choices of  $n$  for the Clustering Emergent Dark Energy model with  $c_s^2 = 0$  using Primary Planck 2018 CMB data. We also show the constraints for the  $\Lambda$ CDM model for comparison.

In all cases we considered  $c_s^2 = 1$ . It is evident from the Fig. 6 that in canonical emergent dark energy scenarios  $H_0$  and  $S_8$  are rather insensitive to  $n$ , and that  $a_t$  is constrained. Comparing to  $\Lambda$ CDM the model infers a higher value for  $H_0$  and a lower one for  $S_8$ .

## B. Clustering Emergent Dark Energy Cosmology

In this section, we explore the impact of clustering Emergent Dark Energy Cosmologies, which corresponds to  $c_s = 0$  on various data sets. The parameter constraints at the 68% confidence level (CL) are presented in the Table III, alongside the best-fit  $\chi^2$  and  $\Delta\chi^2$  assuming  $\Lambda$ CDM.

We observe an increase in the derived values of  $H_0$  and  $S_8$  compared to the Primary Planck 2018 CMB data analysis. Hence, while there is a marginal improvement in the  $H_0$  value, the  $S_8$  value worsens in comparison to the canonical emergent dark energy cosmologies using Primary Planck 2018 CMB data. Because in this model DE can cluster, we find an increment in  $\sigma_8 = 0.838^{+0.033}_{-0.0057}$ . This increase in  $\sigma_8$  is solely responsible for the worsening of the  $S_8$  tension. The model parameters  $10^2 a_t$  and  $n$  (or  $c_{a_0}^2$ ) are reported as  $3.288^{+0.033}_{-0.12}$  and  $< 3.17$  ( $-0.14^{+0.38}_{-0.50}$ ), respectively.

Next, we examine the consequences of considering other data sets within this scenario.

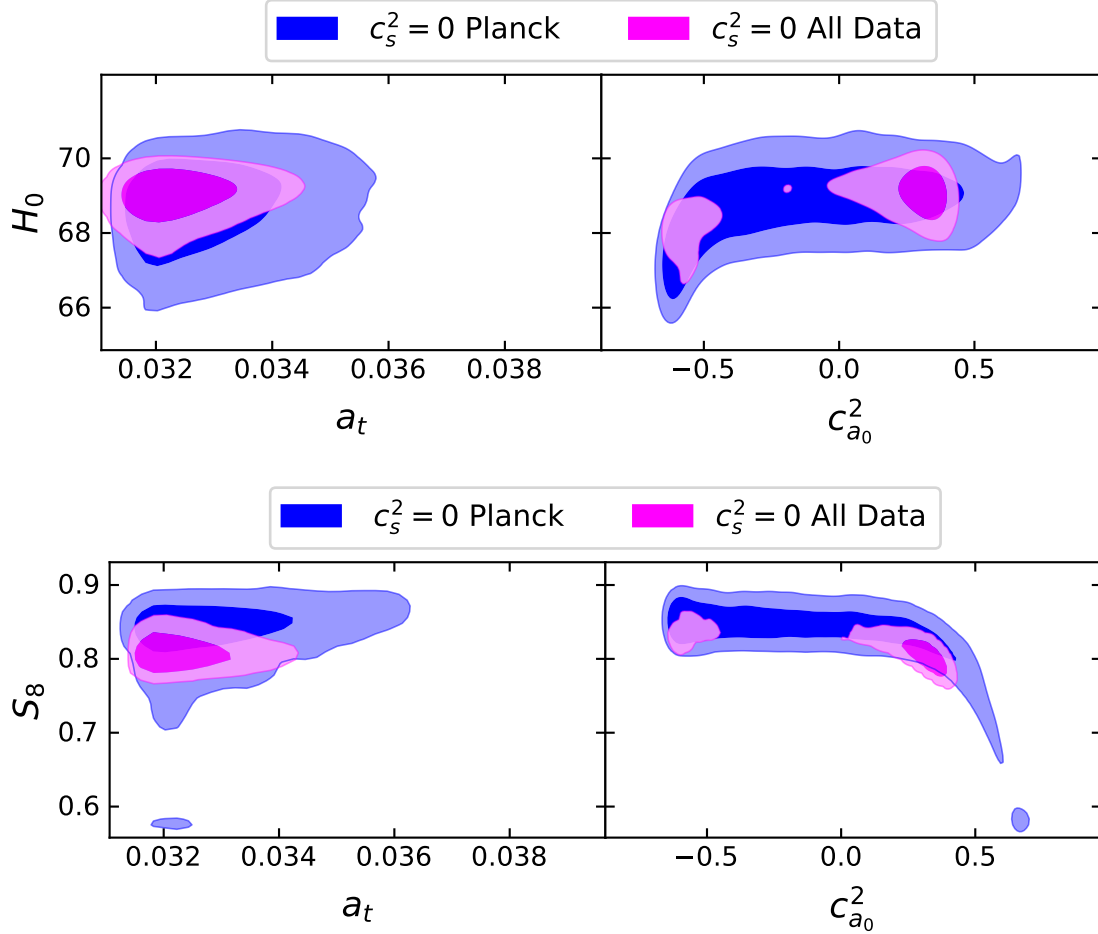


FIG. 8: 2-dimensional marginalized posterior distributions for model parameters  $a_t$  and  $c_{a_0}^2$  (and hence  $n$ ) with  $H_0$  and  $S_8$  in upper and lower panels for clustering emergent dark energy model. These plots show the correlation between model parameters with  $H_0$  and  $S_8$ . The blue and magenta correspond to Primary Planck 2018 CMB data and All data sets described in section III

The present values of the Hubble parameter  $H_0$  and the amplitude of matter fluctuations  $S_8$  follow the same trends across different data sets and their combinations. The inferred values of  $H_0$  and  $S_8$  lie within the ranges of  $[68 - 69]$  km/sec/Mpc and  $[0.843 - 0.808]$ , respectively, for the other combinations. The predictions of the model, represented by  $a_t$  and  $n$  (or the derived parameter  $c_{a_0}^2$ ), reveal a transition redshift  $a_t$  of approximately 0.034. However, in the case of the combination data sets, we find a lower bound on  $n < 3.0$ , indicating the presence of gradient or ghost instabilities in clustering dark energy. The possible correlations between additional model parameters and  $H_0$  and  $S_8$  are illustrated in Fig. 8. The 68 % constraint for different  $n$  are shown in Appendix B, Tables X to XIV.

Finally, we conclude the discussion on clustering in emergent dark energy by commenting on the  $\chi^2$  and  $\Delta\chi^2$ . In this scenario, we observe a worse fit to the data compared to our baseline model  $\Lambda$ CDM and the canonical emergent dark energy case. As mentioned earlier, while it is possible to alleviate the Hubble tension in this scenario, the tension related to large-scale structure becomes more pronounced.

**The mean  $\pm 1\sigma$  constraints for clustering emergent dark energy ( $c_s^2 = 0$ ) model**

Parameter	Planck 2018 CMB	CBSH	CBSHDK	CBSDK
$H_0$	$68.7^{+1.0}_{-0.78}$	$68.61^{+0.67}_{-0.41}$	$69.00^{+0.53}_{-0.34}$	$68.96 \pm 0.40$
$\sigma_8$	$0.838^{+0.023}_{-0.0057}$	$0.846^{+0.012}_{-0.0093}$	$0.814^{+0.014}_{-0.016}$	$0.8422^{+0.0052}_{-0.0070}$
$S_8$	$0.837^{+0.030}_{-0.011}$	$0.846^{+0.014}_{-0.012}$	$0.808^{+0.013}_{-0.018}$	$0.8369^{+0.0084}_{-0.096}$
$\Omega_m$	$0.2993^{+0.0093}_{-0.011}$	$0.3001^{+0.0049}_{-0.0068}$	$0.2958^{+0.0042}_{-0.0057}$	$0.2963^{+0.0044}_{-0.0051}$
$10^2 a_t$	$3.288^{+0.033}_{-0.12}$	$3.255^{+0.022}_{-0.092}$	$3.239^{+0.017}_{-0.077}$	$3.400^{+0.069}_{-0.23}$
$c_s^2$	0	0	0	0
$n$	$< 3.17$	$< 3.14$	$3.67^{+0.47}_{+0.12}$	$> 3.07$
$c_{a_0}^2$	$-0.14^{+0.39}_{-0.50}$	$-0.16 \pm 0.30$	$0.225^{+0.16}_{+0.039}$	$0.28^{+0.64}_{-0.32}$
$\#\sigma_{H_0}$	3.00	3.58	3.46	3.66
$\#\sigma_{S_8}$	2.41	2.61	1.61	0.96
Total $\chi^2$	2767.1379	3852.2095	3859.1056	3857.8257
$\Delta\chi^2$	2.9679	-1.8185	-0.7062	+11.74

TABLE III: The mean  $\pm 1\sigma$  constraints on the cosmological parameters inferred from the various datasets for clustering emergent dark energy ( $c_s^2 = 0$ ) model

### C. Non-canonical Emergent Dark Energy

Finally, we investigate the implications of non-canonical emergent dark energy by allowing the effective sound speed ( $c_s^2$ ) to vary between 0 to 1, along with other model parameters. We present the parameter constraints for this case in Table IV. Similar to previous cases, we find an increase in the value of  $H_0$  and a marginal decrease in  $S_8$ . Referring to the results from the Primary Planck 2018 Cosmic Microwave Background (CMB) analysis, we infer  $H_0 = 68.30^{+0.51}_{-0.72}$  km/sec/Mpc and  $S_8 = 0.822 \pm 0.017$ . The amplitude of matter fluctuations

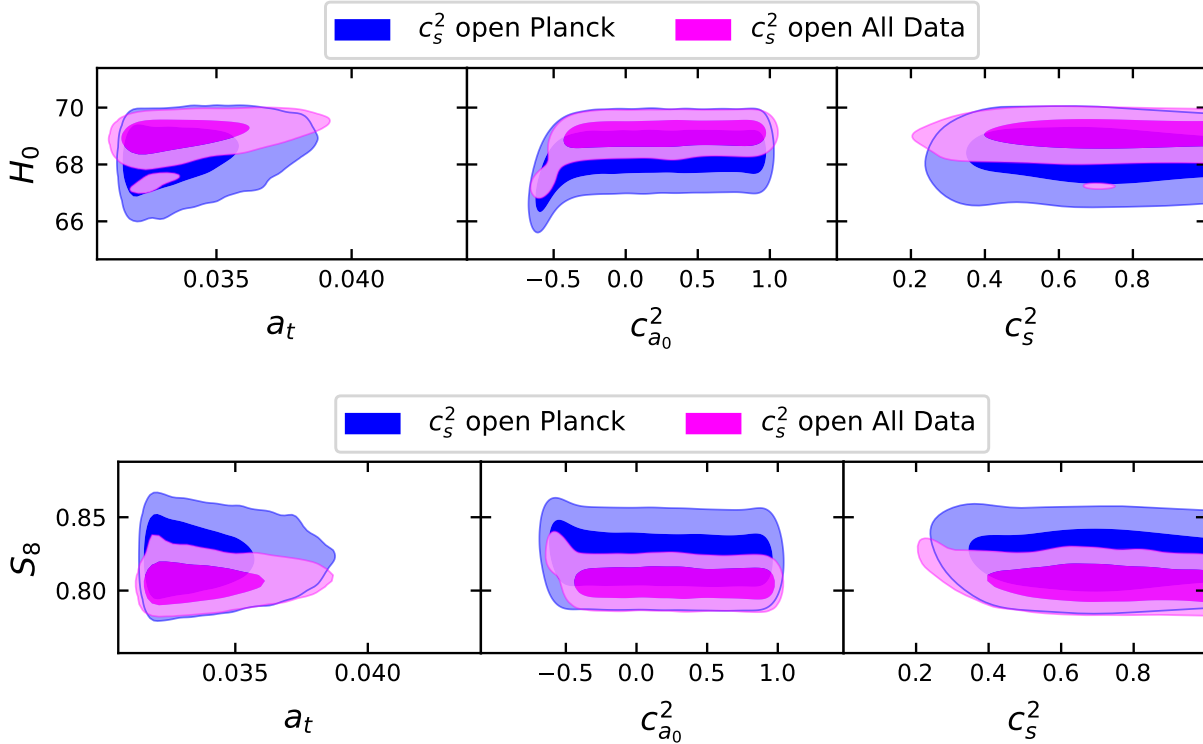


FIG. 9: 2-dimensional marginalized posterior distributions for model parameters  $a_t$  and  $c_{a_0}^2$  (and hence  $n$ ) with  $H_0$  and  $S_8$  in upper and lower panels for non-canonical emergent dark energy model. These plots show the correlation between model parameters with  $H_0$  and  $S_8$ . The blue and magenta correspond to Primary Planck 2018 CMB data and All data sets described in section III

$\sigma_8$  and matter density  $\Omega_m$  are constrained to be  $0.8133 \pm 0.0093$  and  $0.3066_{-0.010}^{+0.0089}$  respectively. The tension metrics for  $H_0$  and  $S_8$  show an improvement of approximately  $1 \sigma$  and  $0.5\sigma$  respectively. Moving to other data sets, the improvement in  $H_0$  and  $S_8$  remains consistent, resulting in a range of  $H_0 \approx 68.8$  km/sec/Mpc and  $S_8 \approx 0.81$ .

In all cases considered, we find the transition scale factor to be approximately  $a_t = 0.034$ , regardless of the data set used. The steepness parameter  $n$  is constrained to ensure that  $c_a^2$  remains free from gradient/ghost instabilities and subluminal throughout the evolution. Using the Primary Planck 2018 CMB data in combination with Baryon Acoustic Oscillations (BAO), Supernovae (SNe), and for the SH0ES measurement, we find that  $n = 3.8_{-1.1}^{+1.8}$  and, consequently,  $c_{a_0}^2 = 0.26_{-0.43}^{+0.62}$ . The effective sound speed of perturbations,  $c_s^2$ , is determined to be  $0.27 \pm 0.46$  for the same data set. The correlation between the model parameters ( $a_t$ ,  $c_{a_0}^2$ , and  $c_s^2$ ) with  $H_0$  and  $S_8$  is depicted in Fig. 9, demonstrating that  $H_0$  and  $S_8$  are

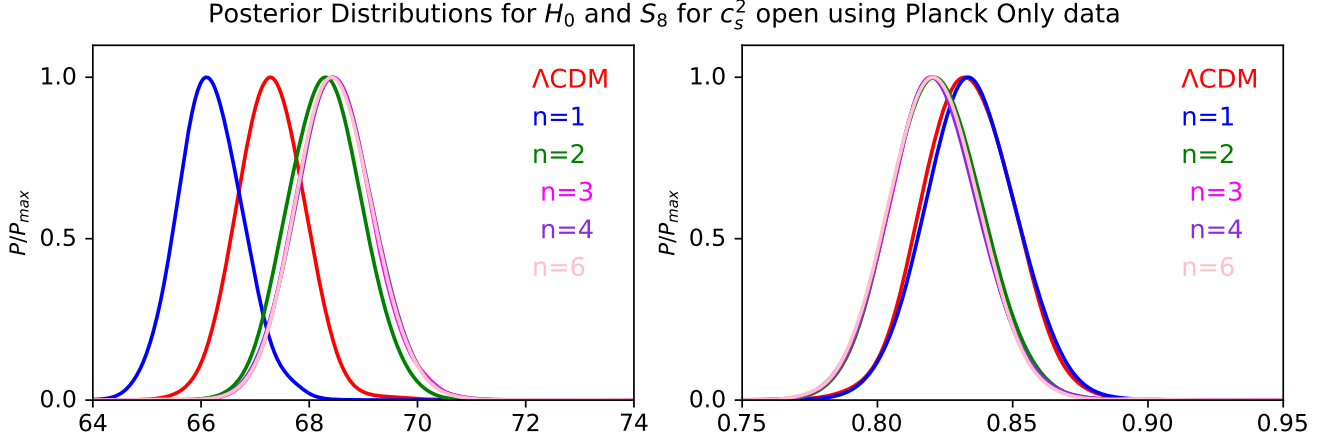


FIG. 10: Normalized posterior distributions for  $H_0$  (in km/sec/Mpc) and  $S_8$  in left and right panels respectively for different choices of  $n$  for Emergent Dark Energy model with keeping  $c_s^2$  open using Primary Planck 2018 CMB data. We also show the constraints for the  $\Lambda$ CDM model also for comparison.

insensitive to the values of  $n$ ,  $c_{a_0}^2$ , and  $c_s^2$ . The non-canonical emergent dark energy model provides a better fit to the data, regardless of the data sets considered. The difference in  $\chi^2$  compared to the  $\Lambda$ CDM model ranges from -3 to -0.20.

Next, we explore the impact of different values of  $n$  in this scenario. Fig. 10 displays the 1-dimensional normalized probability distribution for  $H_0$  and  $S_8$  for  $n$  ranging from 1 to 6, using the Primary Planck 2018 CMB data. For  $n = 1$ , the model is disfavored as it yields  $\Delta\chi^2 \in [2, 13]$  and predicts a lower  $H_0$  and slightly higher value of  $S_8$ . As observed in the case of open  $n$ , for  $n \in [3, 6]$ , we find an improvement in both  $H_0$  and  $S_8$  simultaneously, providing a better fit compared to the  $\Lambda$ CDM model and cases with  $c_s^2 = 1$  or 0. The 68 % constraint for different  $n$  are shown in Appendix C Tables XV to XIX.

We compare all three models analyzed in this paper with  $\Lambda$ CDM in Fig. 11. The Primary Planck 2018 CMB constraints for  $\Lambda$ CDM, and Emergent DE model with  $c_s^2 = 1$ ,  $c_s^2 = 0$  and  $c_s^2$  open are denoted as blue red, magenta, and green respectively. The shaded dark and light regions correspond to the 68% and 95% confidence levels. respectively. We also compare the results with the latest local SH0ES and DES-Y1 measurements. It is clear from both the left and right panels of Fig. 11 that canonical and non-canonical dark energy models offer a marginal increase in values of  $H_0$  and a marginal decrease in  $S_8$ .

**The mean  $\pm 1\sigma$  constraints for non-canonical emergent dark energy (open  $c_s^2$ ) model**

Parameter	Planck 2018 CMB	CBSH	CBSHDK	CBSDK
$H_0$	$68.30^{+0.84}_{-0.72}$	$68.82^{+0.45}_{-0.39}$	$69.00^{+0.48}_{-0.32}$	$68.73 \pm 0.41$
$\sigma_8$	$0.8133 \pm 0.0093$	$0.8147^{+0.0066}_{-0.0080}$	$0.8092^{+0.0059}_{-0.0070}$	$0.8086^{+0.0060}_{-0.0069}$
$S_8$	$0.822 \pm 0.017$	$0.8155^{+0.0091}_{-0.011}$	$0.8063^{+0.0079}_{-0.010}$	$0.8098 \pm 0.0093$
$\Omega_m$	$0.3066^{+0.0089}_{-0.010}$	$0.3006^{+0.0045}_{-0.0052}$	$0.2979^{+0.0036}_{-0.0055}$	$0.3009 \pm 0.0046$
$10^2 a_t$	$3.374^{+0.056}_{-0.21}$	$3.423^{+0.082}_{-0.25}$	$3.381^{+0.061}_{-0.21}$	$3.338^{+0.045}_{-0.17}$
$c_s^2$	$0.65^{+0.26}_{-0.17}$	$0.66^{+0.22}_{-0.19}$	$0.68^{+0.26}_{-0.14}$	$> 0.597$
$n$	$3.45 \pm 1.45$	$3.8^{+1.8}_{-1.1}$	$> 2.95$	$> 3.06$
$c_{a_0}^2$	$0.15 \pm 0.48$	$0.26^{+0.62}_{-0.43}$	$0.24 \pm 0.44$	$0.27 \pm 0.46$
$\#\sigma_{H_0}$	3.54	3.72	3.52	3.85
$\#\sigma_{S_8}$	1.95	1.89	1.68	1.77
Total $\chi^2$	2765.8647	3851.7445	3856.9329	3846.0359
$\Delta\chi^2$	1.6947	-2.2835	-2.8789	-0.0414

TABLE IV: The mean  $\pm 1\sigma$  constraints on the cosmological parameters inferred from the various datasets for non-canonical emergent dark energy (open  $c_s^2$ ) model.

## V. CONCLUSIONS

We have studied the emergent dark energy model by considering the phenomenological fluid approach. This approach offers to probe the arbitrary sound speed of dark energy perturbations. The emergent dark energy behaves like a cosmological constant ( $\Lambda$ ) at late times and asymptotes to a radiation fluid at early times. As such, it incorporates a tracking mechanism and allows for a rather sudden transition in the DE eos. We employed a phenomenological fluid with 2 parameters to mimic this feature. These two parameters are the scale factor, at which the equation of state of the phenomenological fluid crosses 0,  $a_t$ , and the steepness parameter  $n$ . In addition to these parameters, we also have an arbitrary sound speed of dark energy perturbations  $c_s^2$  taking values within the range of 0 to 1. In this paper, we considered the three different case of  $c_s^2 = 1$ ,  $c_s^2 = 0$  and  $c_s^2$  open which we assign them as canonical, clustering and non-canonical emergent dark energy models. The consideration of each case is capable of explaining the current accelerated expansion of the Universe. The

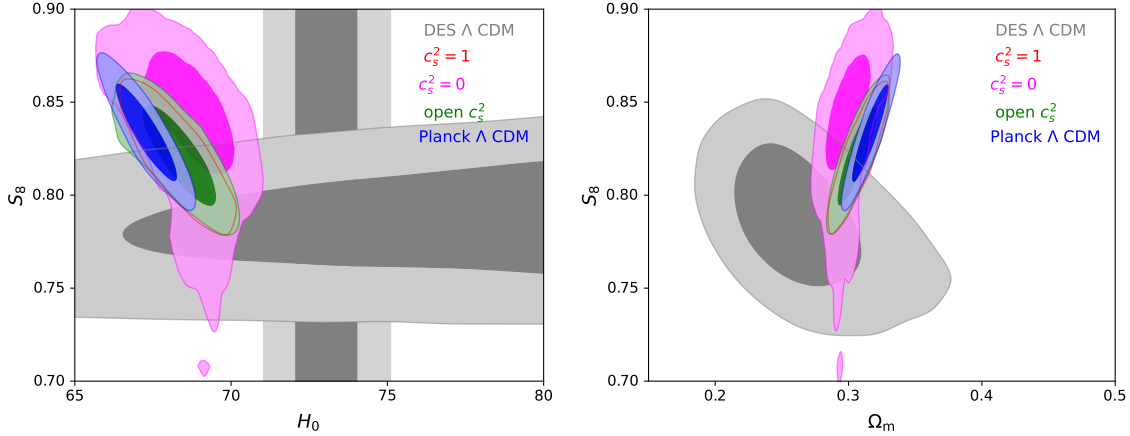


FIG. 11: Left Panel: Comparison of  $H_0$  and  $S_8$  for the  $\Lambda$ CDM and Emergent Dark Energy with different  $c_s^2$ . The horizontal and vertical axis represent the  $H_0$  in units of km/sec/Mpc and  $S_8$  respectively. We denote as  $\Lambda$ CDM as blue,  $c_s^2 = 1$  as red,  $c_s^2 = 0$  as magenta and  $c_s^2$  open as green. The dark and light shaded regions correspond to the 68 % and 95 % confidence level (CL) respectively. Right Panel: Comparison of  $\Omega_m$  and  $S_8$  as horizontal and vertical axis respectively with similar color codes. In both plots the local SH0ES and DES measurements are expressed in gray.

model further offers a built-in solution to the cosmic coincidence problem. We show the impact of  $a_t$  and  $n$  on background and perturbation evolution. The background behavior is illustrated in Fig. 1 and Fig. 2. We notice that there exist a threshold value of  $a_t$  in order to get an era of matter domination for structure formation. The adiabatic sound speed  $c_a^2$  which depends on both parameter  $a_t$  and  $n$  is shown in Fig. 4. It is worth mentioning that  $c_a^2$  has strong dependence on  $n$ . Left panel of Fig. 4 clearly shows that for  $n \geq 3$ ,  $c_a^2$  lies with in range of  $[0, 1]$  further constraining the parameter space.

We then analyze the parameter constraints using the different cosmic data-sets. The aim of this exercise is to check the ability of alleviating the cosmological tensions ( $H_0$  and  $S_8$ ) in the emergent dark energy scenario. We consider the various data-sets to assess the impact of model in reducing the cosmic tensions. We notice an overall improvement of both tensions for all models considered. Out of all the model considered in our analysis, we find that keeping  $c_s^2$  open i.e. non-canonical emergent dark energy provides the best improvement with respect to  $\Lambda$ CDM. The canonical model also reduces both cosmic tensions while clustering (non-relativistic) model reduces the Hubble constant tension and worsens the LSS tension.

During our analysis, we chose a wide prior on  $n \in [1, 6]$ , being agnostic about the fact that  $n \leq 3$  makes the evolution problematic and let the data decide to constrain the value of  $n$ . Interestingly, we find that most of the data-sets constrain the value of  $n$  respecting the theoretical arguments and prefer  $n \geq 3$ . The reduction in the Hubble and LSS tension is rather mild and not very significant statistically. This is probably a reflection of the fact that  $H_0$  and  $S_8$  seem rather insensitive to  $a_t$  and  $n$ . The main difference in the current analysis compared to the emergent unparticles DE model (UDE) [149] is that here the adiabatic speed of sound  $c_a^2$  and the effective sound speed  $c_s^2$  were different, while in the UDE they were equal. Given that in the UDE we got a much more significant reduction of the tensions in a statistically significant way, highlights the important role the adiabatic and effective sound speeds play in inferring the cosmological parameters. Given the insensitivity to  $n$  it seems that fixing  $n$  and  $c_s^2$  and leaving only  $a_t$  as a free parameter can be competitive with the  $\Lambda$ CDM model, and can be constrained significantly with current and future data. The most intriguing result in our opinion is the fact that the transition redshift is highly limited with  $29 < 1 + z < 30$ . As a result one can think of ways to try and detect such a transition.

### Acknowledgements

We acknowledge the Ariel HPC Center at Ariel University for providing computing resources that have contributed to the research results reports reported within this paper.

- 
- [1] PLANCK collaboration, N. Aghanim et al., *Planck 2018 results. VIII. Gravitational lensing, Astron. Astrophys.* **641** (2020) A8 [1807.06210].
  - [2] PLANCK collaboration, N. Aghanim et al., *Planck 2018 results. VI. Cosmological parameters, Astron. Astrophys.* **641** (2020) A6 [1807.06209].
  - [3] PLANCK collaboration, N. Aghanim et al., *Planck 2018 results. V. CMB power spectra and likelihoods, Astron. Astrophys.* **641** (2020) A5 [1907.12875].
  - [4] PAN-STARRS1 collaboration, D. M. Scolnic et al., *The Complete Light-curve Sample of Spectroscopically Confirmed SNe Ia from Pan-STARRS1 and Cosmological Constraints from the Combined Pantheon Sample, Astrophys. J.* **859** (2018) 101 [1710.00845].

- [5] DES collaboration, T. M. C. Abbott et al., *Dark Energy Survey Year 3 results: Cosmological constraints from galaxy clustering and weak lensing*, *Phys. Rev. D* **105** (2022) 023520 [2105.13549].
- [6] H. Hildebrandt et al., *KiDS-450: Cosmological parameter constraints from tomographic weak gravitational lensing*, *Mon. Not. Roy. Astron. Soc.* **465** (2017) 1454 [1606.05338].
- [7] H. Hildebrandt et al., *KiDS+VIKING-450: Cosmic shear tomography with optical and infrared data*, *Astron. Astrophys.* **633** (2020) A69 [1812.06076].
- [8] HSC collaboration, C. Hikage et al., *Cosmology from cosmic shear power spectra with Subaru Hyper Suprime-Cam first-year data*, *Publ. Astron. Soc. Jap.* **71** (2019) 43 [1809.09148].
- [9] A. J. Ross, L. Samushia, C. Howlett, W. J. Percival, A. Burden and M. Manera, *The clustering of the SDSS DR7 main Galaxy sample – I. A 4 per cent distance measure at  $z = 0.15$* , *Mon. Not. Roy. Astron. Soc.* **449** (2015) 835 [1409.3242].
- [10] F. Beutler, C. Blake, M. Colless, D. H. Jones, L. Staveley-Smith, L. Campbell et al., *The 6dF Galaxy Survey: Baryon Acoustic Oscillations and the Local Hubble Constant*, *Mon. Not. Roy. Astron. Soc.* **416** (2011) 3017 [1106.3366].
- [11] BOSS collaboration, S. Alam et al., *The clustering of galaxies in the completed SDSS-III Baryon Oscillation Spectroscopic Survey: cosmological analysis of the DR12 galaxy sample*, *Mon. Not. Roy. Astron. Soc.* **470** (2017) 2617 [1607.03155].
- [12] J. E. Bautista et al., *The Completed SDSS-IV extended Baryon Oscillation Spectroscopic Survey: measurement of the BAO and growth rate of structure of the luminous red galaxy sample from the anisotropic correlation function between redshifts 0.6 and 1*, *Mon. Not. Roy. Astron. Soc.* **500** (2020) 736 [2007.08993].
- [13] H. Gil-Marín et al., *The Completed SDSS-IV extended Baryon Oscillation Spectroscopic Survey: measurement of the BAO and growth rate of structure of the luminous red galaxy sample from the anisotropic power spectrum between redshifts 0.6 and 1.0*, *Mon. Not. Roy. Astron. Soc.* **498** (2020) 2492 [2007.08994].
- [14] eBOSS collaboration, S. Alam et al., *Completed SDSS-IV extended Baryon Oscillation Spectroscopic Survey: Cosmological implications from two decades of spectroscopic surveys at the Apache Point Observatory*, *Phys. Rev. D* **103** (2021) 083533 [2007.08991].
- [15] R. Neveux et al., *The completed SDSS-IV extended Baryon Oscillation Spectroscopic*

- Survey: BAO and RSD measurements from the anisotropic power spectrum of the quasar sample between redshift 0.8 and 2.2*, *Mon. Not. Roy. Astron. Soc.* **499** (2020) 210 [2007.08999].
- [16] J. Hou et al., *The Completed SDSS-IV extended Baryon Oscillation Spectroscopic Survey: BAO and RSD measurements from anisotropic clustering analysis of the Quasar Sample in configuration space between redshift 0.8 and 2.2*, *Mon. Not. Roy. Astron. Soc.* **500** (2020) 1201 [2007.08998].
- [17] H. du Mas des Bourboux et al., *The Completed SDSS-IV Extended Baryon Oscillation Spectroscopic Survey: Baryon Acoustic Oscillations with Ly $\alpha$  Forests*, *Astrophys. J.* **901** (2020) 153 [2007.08995].
- [18] L. A. Escamilla, W. Giarè, E. Di Valentino, R. C. Nunes and S. Vagnozzi, *The state of the dark energy equation of state circa 2023*, 2307.14802.
- [19] S. Weinberg, *The Cosmological Constant Problem*, *Rev. Mod. Phys.* **61** (1989) 1.
- [20] I. Ben-Dayan, M. Hadad and A. Michaelis, *The grand canonical Multiverse and the small cosmological constant*, *JCAP* **09** (2022) 052 [2110.06249].
- [21] I. Ben-Dayan, R. Richter, F. Ruehle and A. Westphal, *Vacuum energy sequestering and conformal symmetry*, *JCAP* **05** (2016) 002 [1507.04158].
- [22] P. J. E. Peebles and B. Ratra, *The Cosmological Constant and Dark Energy*, *Rev. Mod. Phys.* **75** (2003) 559 [astro-ph/0207347].
- [23] S. M. Carroll, W. H. Press and E. L. Turner, *The Cosmological constant*, *Ann. Rev. Astron. Astrophys.* **30** (1992) 499.
- [24] S. M. Carroll, *The Cosmological constant*, *Living Rev. Rel.* **4** (2001) 1 [astro-ph/0004075].
- [25] S. Weinberg, *The Cosmological constant problems*, in *4th International Symposium on Sources and Detection of Dark Matter in the Universe (DM 2000)*, pp. 18–26, 2, 2000, astro-ph/0005265.
- [26] V. Sahni, *The Cosmological constant problem and quintessence*, *Class. Quant. Grav.* **19** (2002) 3435 [astro-ph/0202076].
- [27] T. Padmanabhan, *Cosmological constant: The Weight of the vacuum*, *Phys. Rept.* **380** (2003) 235 [hep-th/0212290].
- [28] S. Nobbenhuis, *Categorizing different approaches to the cosmological constant problem*, *Found. Phys.* **36** (2006) 613 [gr-qc/0411093].

- [29] J. Polchinski, *The Cosmological Constant and the String Landscape*, in *23rd Solway Conference in Physics: The Quantum Structure of Space and Time*, pp. 216–236, 3, 2006, hep-th/0603249.
- [30] E. J. Copeland, M. Sami and S. Tsujikawa, *Dynamics of dark energy*, *Int. J. Mod. Phys. D* **15** (2006) 1753 [hep-th/0603057].
- [31] E. Oks, *Brief review of recent advances in understanding dark matter and dark energy*, *New Astron. Rev.* **93** (2021) 101632 [2111.00363].
- [32] D. Huterer et al., *Growth of Cosmic Structure: Probing Dark Energy Beyond Expansion*, *Astropart. Phys.* **63** (2015) 23 [1309.5385].
- [33] G. Caldera-Cabral, R. Maartens and B. M. Schaefer, *The Growth of Structure in Interacting Dark Energy Models*, *JCAP* **07** (2009) 027 [0905.0492].
- [34] F. Ferlito, S. Vagnozzi, D. F. Mota and M. Baldi, *Cosmological direct detection of dark energy: Non-linear structure formation signatures of dark energy scattering with visible matter*, *Mon. Not. Roy. Astron. Soc.* **512** (2022) 1885 [2201.04528].
- [35] R. C. Nunes and S. Vagnozzi, *Arbitrating the S8 discrepancy with growth rate measurements from redshift-space distortions*, *Mon. Not. Roy. Astron. Soc.* **505** (2021) 5427 [2106.01208].
- [36] M. Chevallier and D. Polarski, *Accelerating universes with scaling dark matter*, *Int. J. Mod. Phys. D* **10** (2001) 213 [gr-qc/0009008].
- [37] E. V. Linder, *Exploring the expansion history of the universe*, *Phys. Rev. Lett.* **90** (2003) 091301 [astro-ph/0208512].
- [38] H. K. Jassal, J. S. Bagla and T. Padmanabhan, *Observational constraints on low redshift evolution of dark energy: How consistent are different observations?*, *Phys. Rev. D* **72** (2005) 103503 [astro-ph/0506748].
- [39] E. M. Barboza, Jr. and J. S. Alcaniz, *A parametric model for dark energy*, *Phys. Lett. B* **666** (2008) 415 [0805.1713].
- [40] B. F. Gerke and G. Efstathiou, *Probing quintessence: Reconstruction and parameter estimation from supernovae*, *Mon. Not. Roy. Astron. Soc.* **335** (2002) 33 [astro-ph/0201336].
- [41] L. A. Escamilla, O. Akarsu, E. Di Valentino and J. A. Vazquez, *Model-independent reconstruction of the Interacting Dark Energy Kernel: Binned and Gaussian process*, 2305.16290.

- [42] S. A. Adil, M. R. Gangopadhyay, M. Sami and M. K. Sharma, *Late-time acceleration due to a generic modification of gravity and the Hubble tension*, *Phys. Rev. D* **104** (2021) 103534 [2106.03093].
- [43] A. Aviles, C. Gruber, O. Luongo and H. Quevedo, *Cosmography and constraints on the equation of state of the Universe in various parametrizations*, *Phys. Rev. D* **86** (2012) 123516 [1204.2007].
- [44] R. K. Sharma, K. L. Pandey and S. Das, *Implications of an Extended Dark Energy Model with Massive Neutrinos*, *Astrophys. J.* **934** (2022) 113 [2202.01749].
- [45] H. E. S. Velten, R. F. vom Marttens and W. Zimdahl, *Aspects of the cosmological “coincidence problem”*, *Eur. Phys. J. C* **74** (2014) 3160 [1410.2509].
- [46] P. J. Steinhardt, L.-M. Wang and I. Zlatev, *Cosmological tracking solutions*, *Phys. Rev. D* **59** (1999) 123504 [astro-ph/9812313].
- [47] I. Zlatev, L.-M. Wang and P. J. Steinhardt, *Quintessence, cosmic coincidence, and the cosmological constant*, *Phys. Rev. Lett.* **82** (1999) 896 [astro-ph/9807002].
- [48] A. Barreira and P. P. Avelino, *Anthropic versus cosmological solutions to the coincidence problem*, *Phys. Rev. D* **83** (2011) 103001 [1103.2401].
- [49] L. Amendola, *Coupled quintessence*, *Phys. Rev. D* **62** (2000) 043511 [astro-ph/9908023].
- [50] A. G. Riess et al., *A 2.4% Determination of the Local Value of the Hubble Constant*, *Astrophys. J.* **826** (2016) 56 [1604.01424].
- [51] A. G. Riess, S. Casertano, D. Kenworthy, D. Scolnic and L. Macri, *Seven Problems with the Claims Related to the Hubble Tension in arXiv:1810.02595*, 1810.03526.
- [52] A. G. Riess, S. Casertano, W. Yuan, L. M. Macri and D. Scolnic, *Large Magellanic Cloud Cepheid Standards Provide a 1% Foundation for the Determination of the Hubble Constant and Stronger Evidence for Physics beyond  $\Lambda$ CDM*, *Astrophys. J.* **876** (2019) 85 [1903.07603].
- [53] A. G. Riess, S. Casertano, W. Yuan, J. B. Bowers, L. Macri, J. C. Zinn et al., *Cosmic Distances Calibrated to 1% Precision with Gaia EDR3 Parallaxes and Hubble Space Telescope Photometry of 75 Milky Way Cepheids Confirm Tension with  $\Lambda$ CDM*, *Astrophys. J. Lett.* **908** (2021) L6 [2012.08534].
- [54] A. G. Riess et al., *A Comprehensive Measurement of the Local Value of the Hubble Constant with  $1\text{kms}^{-1}\text{Mpc}^{-1}$  Uncertainty from the Hubble Space Telescope and the SH0ES*

- Team, Astrophys. J. Lett.* **934** (2022) L7 [2112.04510].
- [55] W. L. Freedman, *Cosmology at a Crossroads*, *Nat. Astron.* **1** (2017) 0121 [1706.02739].
- [56] W. L. Freedman et al., *The Carnegie-Chicago Hubble Program. VIII. An Independent Determination of the Hubble Constant Based on the Tip of the Red Giant Branch*, *Astrophys. J.* **882** (2019) 34 [1907.05922].
- [57] W. L. Freedman, B. F. Madore, T. Hoyt, I. S. Jang, R. Beaton, M. G. Lee et al., *Calibration of the Tip of the Red Giant Branch (TRGB)*, 2002.01550.
- [58] W. L. Freedman, *Measurements of the Hubble Constant: Tensions in Perspective*, *Astrophys. J.* **919** (2021) 16 [2106.15656].
- [59] D. Camarena and V. Marra, *The tension in the absolute magnitude of Type Ia supernovae*, 2307.02434.
- [60] D. Camarena and V. Marra, *A new method to build the (inverse) distance ladder*, *Mon. Not. Roy. Astron. Soc.* **495** (2020) 2630 [1910.14125].
- [61] D. Camarena and V. Marra, *Impact of the cosmic variance on  $H_0$  on cosmological analyses*, *Phys. Rev.* **D98** (2018) 023537 [1805.09900].
- [62] D. Camarena and V. Marra, *Local determination of the Hubble constant and the deceleration parameter*, *Phys. Rev. Res.* **2** (2020) 013028 [1906.11814].
- [63] A. Aviles, J. Klapp and O. Luongo, *Toward unbiased estimations of the statefinder parameters*, *Phys. Dark Univ.* **17** (2017) 25 [1606.09195].
- [64] L. Verde, T. Treu and A. G. Riess, *Tensions between the Early and the Late Universe*, *Nature Astron.* **3** (2019) 891 [1907.10625].
- [65] E. Di Valentino et al., *Cosmology Intertwined III:  $f\sigma_8$  and  $S_8$* , *Astropart. Phys.* **131** (2021) 102604 [2008.11285].
- [66] M. White et al., *Cosmological constraints from the tomographic cross-correlation of DESI Luminous Red Galaxies and Planck CMB lensing*, *JCAP* **02** (2022) 007 [2111.09898].
- [67] C. Heymans et al., *KiDS-1000 Cosmology: Multi-probe weak gravitational lensing and spectroscopic galaxy clustering constraints*, *Astron. Astrophys.* **646** (2021) A140 [2007.15632].
- [68] DES collaboration, S. Pandey et al., *Dark Energy Survey year 3 results: Constraints on cosmological parameters and galaxy-bias models from galaxy clustering and galaxy-galaxy lensing using the redMaGiC sample*, *Phys. Rev. D* **106** (2022) 043520 [2105.13545].

- [69] C. García-García, J. R. Zapatero, D. Alonso, E. Bellini, P. G. Ferreira, E.-M. Mueller et al., *The growth of density perturbations in the last  $\sim 10$  billion years from tomographic large-scale structure data*, *JCAP* **10** (2021) 030 [2105.12108].
- [70] LSST DARK ENERGY SCIENCE collaboration, E. P. Longley et al., *A Unified Catalog-level Reanalysis of Stage-III Cosmic Shear Surveys*, 2208.07179.
- [71] ACT collaboration, S. Aiola et al., *The Atacama Cosmology Telescope: DR4 Maps and Cosmological Parameters*, 2007.07288.
- [72] S.-F. Chen, M. White, J. DeRose and N. Kokron, *Cosmological analysis of three-dimensional BOSS galaxy clustering and Planck CMB lensing cross correlations via Lagrangian perturbation theory*, *JCAP* **07** (2022) 041 [2204.10392].
- [73] D. Brout et al., *The Pantheon+ Analysis: Cosmological Constraints*, 2202.04077.
- [74] E. Mörtzell and S. Dhawan, *Does the Hubble constant tension call for new physics?*, *JCAP* **09** (2018) 025 [1801.07260].
- [75] M. Kamionkowski and A. G. Riess, *The Hubble Tension and Early Dark Energy*, 2211.04492.
- [76] P. Agrawal, F.-Y. Cyr-Racine, D. Pinner and L. Randall, *Rock 'n' Roll Solutions to the Hubble Tension*, 1904.01016.
- [77] M.-X. Lin, G. Benevento, W. Hu and M. Raveri, *Acoustic Dark Energy: Potential Conversion of the Hubble Tension*, *Phys. Rev. D* **100** (2019) 063542 [1905.12618].
- [78] T. L. Smith, V. Poulin and M. A. Amin, *Oscillating scalar fields and the Hubble tension: a resolution with novel signatures*, *Phys. Rev. D* **101** (2020) 063523 [1908.06995].
- [79] S. Alexander, H. Bernardo and M. W. Toomey, *Addressing the Hubble and  $S_8$  Tensions with a Kinetically Mixed Dark Sector*, 2207.13086.
- [80] L. Knox and M. Millea, *Hubble constant hunter's guide*, *Phys. Rev. D* **101** (2020) 043533 [1908.03663].
- [81] V. I. Sabla and R. R. Caldwell, *No  $H_0$  assistance from assisted quintessence*, *Phys. Rev. D* **103** (2021) 103506 [2103.04999].
- [82] J. Sakstein and M. Trodden, *Early Dark Energy from Massive Neutrinos as a Natural Resolution of the Hubble Tension*, *Phys. Rev. Lett.* **124** (2020) 161301 [1911.11760].
- [83] M. Carrillo González, Q. Liang, J. Sakstein and M. Trodden, *Neutrino-Assisted Early Dark Energy: Theory and Cosmology*, *JCAP* **04** (2021) 063 [2011.09895].

- [84] J. C. Hill, E. McDonough, M. W. Toomey and S. Alexander, *Early dark energy does not restore cosmological concordance*, *Phys. Rev. D* **102** (2020) 043507 [2003.07355].
- [85] M. M. Ivanov, E. McDonough, J. C. Hill, M. Simonović, M. W. Toomey, S. Alexander et al., *Constraining Early Dark Energy with Large-Scale Structure*, *Phys. Rev. D* **102** (2020) 103502 [2006.11235].
- [86] E. Di Valentino and S. Bridle, *Exploring the Tension between Current Cosmic Microwave Background and Cosmic Shear Data*, *Symmetry* **10** (2018) 585.
- [87] A. Cuceu, J. Farr, P. Lemos and A. Font-Ribera, *Baryon Acoustic Oscillations and the Hubble Constant: Past, Present and Future*, *JCAP* **10** (2019) 044 [1906.11628].
- [88] N. Schöneberg, J. Lesgourgues and D. C. Hooper, *The BAO+BBN take on the Hubble tension*, *JCAP* **10** (2019) 029 [1907.11594].
- [89] A. Krolewski and S. Ferraro, *The Integrated Sachs Wolfe effect: unWISE and Planck constraints on dynamical dark energy*, *JCAP* **04** (2022) 033 [2110.13959].
- [90] S. Vagnozzi, *New physics in light of the  $H_0$  tension: An alternative view*, *Phys. Rev. D* **102** (2020) 023518 [1907.07569].
- [91] S. Vagnozzi, A. Loeb and M. Moresco, *Eppur è piatto? The Cosmic Chronometers Take on Spatial Curvature and Cosmic Concordance*, *Astrophys. J.* **908** (2021) 84 [2011.11645].
- [92] S. Vagnozzi, *Consistency tests of  $\Lambda$ CDM from the early integrated Sachs-Wolfe effect: Implications for early-time new physics and the Hubble tension*, *Phys. Rev. D* **104** (2021) 063524 [2105.10425].
- [93] S. Vagnozzi, F. Pacucci and A. Loeb, *Implications for the Hubble tension from the ages of the oldest astrophysical objects*, *JHEAp* **36** (2022) 27 [2105.10421].
- [94] L. Feng, J.-F. Zhang and X. Zhang, *A search for sterile neutrinos with the latest cosmological observations*, *Eur. Phys. J. C* **77** (2017) 418 [1703.04884].
- [95] M. Benetti, L. L. Graef and J. S. Alcaniz, *Do joint CMB and HST data support a scale invariant spectrum?*, *JCAP* **04** (2017) 003 [1702.06509].
- [96] S. Kumar and R. C. Nunes, *Echo of interactions in the dark sector*, *Phys. Rev. D* **96** (2017) 103511 [1702.02143].
- [97] S. Vagnozzi, E. Giusarma, O. Mena, K. Freese, M. Gerbino, S. Ho et al., *Unveiling  $\nu$  secrets with cosmological data: neutrino masses and mass hierarchy*, *Phys. Rev. D* **96** (2017) 123503 [1701.08172].

- [98] G.-B. Zhao et al., *Dynamical dark energy in light of the latest observations*, *Nature Astron.* **1** (2017) 627 [1701.08165].
- [99] V. Prilepina and Y. Tsai, *Reconciling Large And Small-Scale Structure In Twin Higgs Models*, *JHEP* **09** (2017) 033 [1611.05879].
- [100] Z. Chacko, Y. Cui, S. Hong, T. Okui and Y. Tsai, *Partially Acoustic Dark Matter, Interacting Dark Radiation, and Large Scale Structure*, *JHEP* **12** (2016) 108 [1609.03569].
- [101] P. Ko and Y. Tang, *Residual Non-Abelian Dark Matter and Dark Radiation*, *Phys. Lett. B* **768** (2017) 12 [1609.02307].
- [102] D.-M. Xia and S. Wang, *Constraining interacting dark energy models with latest cosmological observations*, *Mon. Not. Roy. Astron. Soc.* **463** (2016) 952 [1608.04545].
- [103] S. Kumar and R. C. Nunes, *Probing the interaction between dark matter and dark energy in the presence of massive neutrinos*, *Phys. Rev. D* **94** (2016) 123511 [1608.02454].
- [104] T. Karwal and M. Kamionkowski, *Dark energy at early times, the Hubble parameter, and the string axiverse*, *Phys. Rev. D* **94** (2016) 103523 [1608.01309].
- [105] P. Ko and Y. Tang, *Light dark photon and fermionic dark radiation for the Hubble constant and the structure formation*, *Phys. Lett. B* **762** (2016) 462 [1608.01083].
- [106] T. Tram, R. Vallance and V. Vennin, *Inflation Model Selection meets Dark Radiation*, *JCAP* **01** (2017) 046 [1606.09199].
- [107] Q.-G. Huang and K. Wang, *How the dark energy can reconcile Planck with local determination of the Hubble constant*, *Eur. Phys. J. C* **76** (2016) 506 [1606.05965].
- [108] E. Di Valentino, A. Melchiorri and J. Silk, *Reconciling Planck with the local value of  $H_0$  in extended parameter space*, *Phys. Lett. B* **761** (2016) 242 [1606.00634].
- [109] J. Solà Peracaula, J. de Cruz Pérez and A. Gómez-Valent, *Dynamical dark energy vs.  $\Lambda = \text{const}$  in light of observations*, *EPL* **121** (2018) 39001 [1606.00450].
- [110] J. Solà, A. Gómez-Valent and J. de Cruz Pérez, *First evidence of running cosmic vacuum: challenging the concordance model*, *Astrophys. J.* **836** (2017) 43 [1602.02103].
- [111] J. Sola, A. Gomez-Valent and J. de Cruz Pérez, *Hints of dynamical vacuum energy in the expanding Universe*, *Astrophys. J. Lett.* **811** (2015) L14 [1506.05793].
- [112] Z. Berezhiani, A. D. Dolgov and I. I. Tkachev, *Reconciling Planck results with low redshift astronomical measurements*, *Phys. Rev. D* **92** (2015) 061303 [1505.03644].
- [113] R. Wojtak and J. Hjorth, *Intrinsic tension in the supernova sector of the local Hubble*

- constant measurement and its implications, Mon. Not. Roy. Astron. Soc.* **515** (2022) 2790 [2206.08160].
- [114] E. Mortsell, A. Goobar, J. Johansson and S. Dhawan, *The Hubble Tension Revisited: Additional Local Distance Ladder Uncertainties, Astrophys. J.* **935** (2022) 58 [2106.09400].
- [115] E. Mortsell, A. Goobar, J. Johansson and S. Dhawan, *Sensitivity of the Hubble Constant Determination to Cepheid Calibration, Astrophys. J.* **933** (2022) 212 [2105.11461].
- [116] G. Efstathiou, *A Lockdown Perspective on the Hubble Tension (with comments from the SH0ES team)*, 2007.10716.
- [117] J.-P. Hu and F.-Y. Wang, *Hubble Tension: The Evidence of New Physics, Universe* **9** (2023) 94 [2302.05709].
- [118] E. Di Valentino, *Challenges of the Standard Cosmological Model, Universe* **8** (2022) 399.
- [119] E. Abdalla et al., *Cosmology intertwined: A review of the particle physics, astrophysics, and cosmology associated with the cosmological tensions and anomalies, JHEAp* **34** (2022) 49 [2203.06142].
- [120] P. Shah, P. Lemos and O. Lahav, *A buyer's guide to the Hubble constant, Astron. Astrophys. Rev.* **29** (2021) 9 [2109.01161].
- [121] L. Perivolaropoulos and F. Skara, *Challenges for  $\Lambda$ CDM: An update, New Astron. Rev.* **95** (2022) 101659 [2105.05208].
- [122] E. Di Valentino, O. Mena, S. Pan, L. Visinelli, W. Yang, A. Melchiorri et al., *In the realm of the Hubble tension—a review of solutions, Class. Quant. Grav.* **38** (2021) 153001 [2103.01183].
- [123] E. Di Valentino et al., *Snowmass2021 - Letter of interest cosmology intertwined II: The hubble constant tension, Astropart. Phys.* **131** (2021) 102605 [2008.11284].
- [124] E. Di Valentino, A. Melchiorri, O. Mena and S. Vagnozzi, *Interacting dark energy in the early 2020s: A promising solution to the  $H_0$  and cosmic shear tensions, Phys. Dark Univ.* **30** (2020) 100666 [1908.04281].
- [125] E. Di Valentino, A. Melchiorri, O. Mena and S. Vagnozzi, *Nonminimal dark sector physics and cosmological tensions, Phys. Rev. D* **101** (2020) 063502 [1910.09853].
- [126] S. Dhawan, J. Alsing and S. Vagnozzi, *Non-parametric spatial curvature inference using late-Universe cosmological probes, Mon. Not. Roy. Astron. Soc.* **506** (2021) L1 [2104.02485].

- [127] O. H. E. Philcox and M. M. Ivanov, *BOSS DR12 full-shape cosmology:  $\Lambda$ CDM constraints from the large-scale galaxy power spectrum and bispectrum monopole*, *Phys. Rev. D* **105** (2022) 043517 [2112.04515].
- [128] P. Zhang, G. D'Amico, L. Senatore, C. Zhao and Y. Cai, *BOSS Correlation Function analysis from the Effective Field Theory of Large-Scale Structure*, *JCAP* **02** (2022) 036 [2110.07539].
- [129] S. Yuan, L. H. Garrison, D. J. Eisenstein and R. H. Wechsler, *Stringent  $\sigma_8$  constraints from small-scale galaxy clustering using a hybrid MCMC + emulator framework*, *Mon. Not. Roy. Astron. Soc.* **515** (2022) 871 [2203.11963].
- [130] Z. Zhai, J. L. Tinker, A. Banerjee, J. DeRose, H. Guo, Y.-Y. Mao et al., *The Aemulus Project V: Cosmological constraint from small-scale clustering of BOSS galaxies*, 2203.08999.
- [131] T. Simon, P. Zhang, V. Poulin and T. L. Smith, *On the consistency of effective field theory analyses of BOSS power spectrum*, 2208.05929.
- [132] DES collaboration, A. Amon et al., *Dark Energy Survey Year 3 results: Cosmology from cosmic shear and robustness to data calibration*, *Phys. Rev. D* **105** (2022) 023514 [2105.13543].
- [133] J. L. v. d. Busch et al., *KiDS-1000: cosmic shear with enhanced redshift calibration*, 2204.02396.
- [134] PLANCK collaboration, P. A. R. Ade et al., *Planck 2015 results. XXIV. Cosmology from Sunyaev-Zeldovich cluster counts*, *Astron. Astrophys.* **594** (2016) A24 [1502.01597].
- [135] A. Krolewski, S. Ferraro and M. White, *Cosmological constraints from unWISE and Planck CMB lensing tomography*, *JCAP* **12** (2021) 028 [2105.03421].
- [136] N. Schöneberg, G. Franco Abellán, A. Pérez Sánchez, S. J. Witte, V. Poulin and J. Lesgourgues, *The  $H_0$  Olympics: A fair ranking of proposed models*, *Phys. Rept.* **984** (2022) 1 [2107.10291].
- [137] A. Amon and G. Efstathiou, *A non-linear solution to the  $S_8$  tension?*, 2206.11794.
- [138] A. Sarkar and B. Ghosh, *Early Dark Energy Motivated Quintessential  $\alpha$ -Attractor Inflaton Potential*, 2307.00603.
- [139] A. Sarkar and B. Ghosh, *Constraining the quintessential  $\alpha$ -attractor inflation through dynamical horizon exit method*, *Phys. Dark Univ.* **41** (2023) 101239 [2305.00230].

- [140] G. Bargiacchi, M. G. Dainotti and S. Capozziello, *Tensions with the flat  $\Lambda$ CDM model from high-redshift cosmography*, 2307.15359.
- [141] M. G. Dainotti, G. Bargiacchi, M. Bogdan, A. L. Lenart, K. Iwasaki, S. Capozziello et al., *Reducing the Uncertainty on the Hubble Constant up to 35% with an Improved Statistical Analysis: Different Best-fit Likelihoods for Type Ia Supernovae, Baryon Acoustic Oscillations, Quasars, and Gamma-Ray Bursts*, *Astrophys. J.* **951** (2023) 63 [2305.10030].
- [142] G. Bargiacchi, M. Benetti, S. Capozziello, E. Lusso, G. Risaliti and M. Signorini, *Quasar cosmology: dark energy evolution and spatial curvature*, *Mon. Not. Roy. Astron. Soc.* **515** (2022) 1795 [2111.02420].
- [143] G. Bargiacchi, M. G. Dainotti, S. Nagataki and S. Capozziello, *Gamma-Ray Bursts, Quasars, Baryonic Acoustic Oscillations, and Supernovae Ia: new statistical insights and cosmological constraints*, 2303.07076.
- [144] A. L. Lenart, G. Bargiacchi, M. G. Dainotti, S. Nagataki and S. Capozziello, *A Bias-free Cosmological Analysis with Quasars Alleviating  $H_0$  Tension*, *Astrophys. J. Suppl.* **264** (2023) 46 [2211.10785].
- [145] M. G. Dainotti, B. De Simone, T. Schiavone, G. Montani, E. Rinaldi, G. Lambiase et al., *On the Evolution of the Hubble Constant with the SNe Ia Pantheon Sample and Baryon Acoustic Oscillations: A Feasibility Study for GRB-Cosmology in 2030*, *Galaxies* **10** (2022) 24 [2201.09848].
- [146] M. G. Dainotti, B. De Simone, T. Schiavone, G. Montani, E. Rinaldi and G. Lambiase, *On the Hubble constant tension in the SNe Ia Pantheon sample*, *Astrophys. J.* **912** (2021) 150 [2103.02117].
- [147] M. G. Dainotti, G. Bargiacchi, M. Bogdan, S. Capozziello and S. Nagataki, *Reduced uncertainties up to 43% on the Hubble constant and the matter density with the SNe Ia with a new statistical analysis*, 2303.06974.
- [148] A. Reeves, L. Herold, S. Vagnozzi, B. D. Sherwin and E. G. M. Ferreira, *Restoring cosmological concordance with early dark energy and massive neutrinos?*, *Mon. Not. Roy. Astron. Soc.* **520** (2023) 3688 [2207.01501].
- [149] I. Ben-Dayan and U. Kumar, *Emergent Unparticles Dark Energy can restore cosmological concordance*, 2302.00067.
- [150] M. Artymowski, I. Ben-Dayan and U. Kumar, *More on emergent dark energy from*

- unparticles*, *Phys. Rev. D* **106** (2022) 083502 [2111.09946].
- [151] M. Artymowski, I. Ben-Dayan and U. Kumar, *Emergent dark energy from unparticles*, *Phys. Rev. D* **103** (2021) L121303 [2010.02998].
- [152] P. Agrawal, G. Obied and C. Vafa,  *$H_0$  tension, swampland conjectures, and the epoch of fading dark matter*, *Phys. Rev. D* **103** (2021) 043523 [1906.08261].
- [153] C. Vafa, *The String landscape and the swampland*, [hep-th/0509212](#).
- [154] E. Palti, *The Swampland: Introduction and Review*, *Fortsch. Phys.* **67** (2019) 1900037 [1903.06239].
- [155] G. Obied, H. Ooguri, L. Spodyneiko and C. Vafa, *De Sitter Space and the Swampland*, 1806.08362.
- [156] P. Agrawal, G. Obied, P. J. Steinhardt and C. Vafa, *On the Cosmological Implications of the String Swampland*, *Phys. Lett. B* **784** (2018) 271 [1806.09718].
- [157] S. K. Garg and C. Krishnan, *Bounds on Slow Roll and the de Sitter Swampland*, *JHEP* **11** (2019) 075 [1807.05193].
- [158] H. Ooguri, E. Palti, G. Shiu and C. Vafa, *Distance and de Sitter Conjectures on the Swampland*, *Phys. Lett. B* **788** (2019) 180 [1810.05506].
- [159] I. Ben-Dayan, *Draining the Swampland*, *Phys. Rev. D* **99** (2019) 101301 [1808.01615].
- [160] C.-P. Ma and E. Bertschinger, *Cosmological perturbation theory in the synchronous and conformal Newtonian gauges*, *Astrophys. J.* **455** (1995) 7 [astro-ph/9506072].
- [161] J. M. Bardeen, *Gauge-invariant cosmological perturbations*, *Phys. Rev. D* **22** (1980) 1882.
- [162] KILO-DEGREE SURVEY, DES collaboration, T. M. C. Abbott et al., *DES Y3 + KiDS-1000: Consistent cosmology combining cosmic shear surveys*, 2305.17173.
- [163] T. Barreiro, E. J. Copeland and N. J. Nunes, *Quintessence arising from exponential potentials*, *Phys. Rev. D* **61** (2000) 127301 [astro-ph/9910214].
- [164] T. Chiba, A. De Felice and S. Tsujikawa, *Observational constraints on quintessence: thawing, tracker, and scaling models*, *Phys. Rev. D* **87** (2013) 083505 [1210.3859].
- [165] R. R. Caldwell, M. Doran, C. M. Mueller, G. Schafer and C. Wetterich, *Early quintessence in light of WMAP*, *Astrophys. J. Lett.* **591** (2003) L75 [astro-ph/0302505].
- [166] R. R. Caldwell, *An introduction to quintessence*, *Braz. J. Phys.* **30** (2000) 215.
- [167] R. R. Caldwell and M. Doran, *Cosmic microwave background and supernova constraints on quintessence: Concordance regions and target models*, *Phys. Rev. D* **69** (2004) 103517

- [astro-ph/0305334].
- [168] A. Guarnizo, J. B. Orjuela-Quintana and C. A. Valenzuela-Toledo, *Dynamical analysis of cosmological models with non-Abelian gauge vector fields*, *Phys. Rev. D* **102** (2020) 083507 [2007.12964].
- [169] A. Mehrabi, A. Maleknejad and V. Kamali, *Gaugessence: a dark energy model with early time radiation-like equation of state*, *Astrophys. Space Sci.* **362** (2017) 53 [1510.00838].
- [170] L. G. Gomez and Y. Rodriguez, *Coupled multi-Proca vector dark energy*, *Phys. Dark Univ.* **31** (2021) 100759 [2004.06466].
- [171] R. C. Batista, *A Short Review on Clustering Dark Energy*, *Universe* **8** (2021) 22 [2204.12341].
- [172] J. Dakin, S. Hannestad, T. Tram, M. Knabenhans and J. Stadel, *Dark energy perturbations in  $N$ -body simulations*, *JCAP* **08** (2019) 013 [1904.05210].
- [173] F. Hassani, J. Adamek, M. Kunz and F. Vernizzi,  *$k$ -evolution: a relativistic  $N$ -body code for clustering dark energy*, *JCAP* **12** (2019) 011 [1910.01104].
- [174] F. Hassani, J. Adamek and M. Kunz, *Clustering dark energy imprints on cosmological observables of the gravitational field*, *Mon. Not. Roy. Astron. Soc.* **500** (2020) 4514 [2007.04968].
- [175] D. F. Mota and C. van de Bruck, *On the Spherical collapse model in dark energy cosmologies*, *Astron. Astrophys.* **421** (2004) 71 [astro-ph/0401504].
- [176] D. Bertacca, N. Bartolo, A. Diaferio and S. Matarrese, *How the Scalar Field of Unified Dark Matter Models Can Cluster*, *JCAP* **10** (2008) 023 [0807.1020].
- [177] C. Armendariz-Picon, V. F. Mukhanov and P. J. Steinhardt, *Essentials of  $k$  essence*, *Phys. Rev. D* **63** (2001) 103510 [astro-ph/0006373].
- [178] A. Joseph and R. Saha, *Dark energy with oscillatory tracking potential: observational constraints and perturbative effects*, *Mon. Not. Roy. Astron. Soc.* **511** (2022) 1637 [2110.00229].
- [179] S. DeDeo, R. R. Caldwell and P. J. Steinhardt, *Effects of the sound speed of quintessence on the microwave background and large scale structure*, *Phys. Rev. D* **67** (2003) 103509 [astro-ph/0301284].
- [180] J. K. Erickson, R. R. Caldwell, P. J. Steinhardt, C. Armendariz-Picon and V. F. Mukhanov, *Measuring the speed of sound of quintessence*, *Phys. Rev. Lett.* **88** (2002)

- 121301 [astro-ph/0112438].
- [181] R. D'Agostino, O. Luongo and M. Muccino, *Healing the cosmological constant problem during inflation through a unified quasi-quintessence matter field*, *Class. Quant. Grav.* **39** (2022) 195014 [2204.02190].
- [182] O. Luongo and H. Quevedo, *A Unified Dark Energy Model from a Vanishing Speed of Sound with Emergent Cosmological Constant*, *Int. J. Mod. Phys. D* **23** (2014) 1450012.
- [183] J. Torrado and A. Lewis, *Cobaya: Code for Bayesian Analysis of hierarchical physical models*, *JCAP* **05** (2021) 057 [2005.05290].
- [184] A. Lewis, A. Challinor and A. Lasenby, *Efficient computation of CMB anisotropies in closed FRW models*, *Astrophys. J.* **538** (2000) 473 [astro-ph/9911177].
- [185] A. Gelman and D. B. Rubin, *Inference from Iterative Simulation Using Multiple Sequences*, *Statist. Sci.* **7** (1992) 457.

# Appendices

## Appendix A: Canonical Emergent Dark Energy

### A.1. Constraints for Planck 2018 CMB for different values of $n$

The mean  $\pm 1\sigma$  constraints from Planck 2018 CMB for  $c_s^2 = 1$  for different  $n$

Params	$n = 1$	$n = 2$	$n = 3$	$n = 4$	$n = 6$
$H_0$	$66.15 \pm 0.68$	$68.18 \pm 0.87$	$68.42^{+0.68}_{-0.83}$	$68.35 \pm 0.75$	$68.39^{+0.68}_{-0.79}$
$\sigma_8$	$0.7973^{+0.0073}_{-0.0084}$	$0.8122^{+0.0081}_{-0.0097}$	$0.8115 \pm 0.0096$	$0.8120 \pm 0.0094$	$0.8128^{+0.0074}_{-0.0090}$
$S_8$	$0.832 \pm 0.017$	$0.823 \pm 0.021$	$0.819 \pm 0.018$	$0.820 \pm 0.018$	$0.821 \pm 0.017$
$\Omega_m$	$0.3270 \pm 0.0095$	$0.308 \pm 0.011$	$0.3055 \pm 0.0098$	$0.3063 \pm 0.0094$	$0.3059 \pm 0.0094$
$10^2 a_t$	$3.470^{+0.075}_{-0.31}$	$3.429^{+0.056}_{-0.27}$	$3.421^{+0.057}_{-0.26}$	$3.390^{+0.068}_{-0.23}$	$3.417^{+0.051}_{-0.25}$
Total $\chi^2$	2766.0376	2765.8973	2765.8248	2766.1938	2765.7482
$\Delta\chi^2$	1.8676	1.7273	1.6548	2.0238	1.5782

TABLE V: The mean  $\pm 1\sigma$ (best-fit) constraints on the cosmological parameters inferred from the *Planck* 2018 CMB data (including TTEETE) for  $\Lambda$ CDM and Canonical Emergent DE scenario with different values of  $n$  varying from 1 to 6.

### A.2. Planck + Lensing + BAO + $H_0$

The mean  $\pm 1\sigma$  constraints from Planck 2018 + Lensing + BAO + SN +  $H_0$

Parameter	$n = 1$	$n = 2$	$n = 3$	$n = 4$	$n = 6$
$H_0$	$67.33^{+0.67}_{-0.51}$	$68.88^{+0.62}_{-0.89}$	$68.85^{+0.48}_{-0.59}$	$68.96^{+0.49}_{-0.80}$	$68.90^{+0.50}_{-0.60}$
$\sigma_8$	$0.7985^{+0.0065}_{-0.0081}$	$0.8139^{+0.0065}_{-0.0088}$	$0.8141^{+0.0062}_{-0.0082}$	$0.8141^{+0.0063}_{-0.0086}$	$0.8137^{+0.0060}_{-0.0081}$
$S_8$	$0.812^{+0.011}_{-0.015}$	$0.814 \pm 0.016$	$0.8149^{+0.0096}_{-0.012}$	$0.813 \pm 0.014$	$0.814^{+0.010}_{-0.011}$
$\Omega_m$	$0.3105^{+0.0062}_{-0.0092}$	$0.3000^{+0.0091}_{-0.0081}$	$0.3006 \pm 0.0082$	$0.2995^{+0.0084}_{-0.0065}$	$0.3000 \pm 0.0075$
$10^2 a_t$	$3.58^{+0.10}_{-0.41}$	$3.54^{+0.11}_{-0.37}$	$3.500^{+0.089}_{-0.32}$	$3.514^{+0.091}_{-0.35}$	$3.496^{+0.090}_{-0.32}$
Total $\chi^2$	3869.1753	3852.9131	3851.876	3852.3776	3852.1676
$\Delta\chi^2$	15.5434	-1.0037	-1.2103	-0.9626	-1.2265

TABLE VI: The mean  $\pm 1\sigma$ (best-fit) constraints on the cosmological parameters inferred from the *Planck* 2018 CMB data (including TTEETE + lensing), BAO, SNe and SH0ES data for  $\Lambda$ CDM and Canonical Emergent DE scenario with different values of  $n$  varying from 1 to 6.

### A.3. Planck + Lensing + BAO + $H_0$ + DES-Y1

Constraints from Planck 2018 + Lensing + BAO + SN +  $H_0$  + DES for Canonical Emergent DE

Parameter	$n = 1$	$n = 2$	$n = 3$	$n = 4$	$n = 6$	$n$ open
$H_0$	$67.59 \pm 0.64$	$68.75^{+0.51}_{-0.41}$	$68.82^{+0.45}_{-0.40}$	$69.01^{+0.44}_{-0.56}$	$68.99^{+0.45}_{-0.51}$	$68.93^{+0.53}_{-0.41}$
$\sigma_8$	$0.7972^{+0.0064}_{-0.0081}$	$0.8110^{+0.0062}_{-0.0074}$	$0.8117^{+0.0059}_{-0.0073}$	$0.8126^{+0.0061}_{-0.0079}$	$0.8123^{+0.0063}_{-0.0075}$	$0.8107^{+0.0065}_{-0.0075}$
$S_8$	$0.8063^{+0.0095}_{-0.012}$	$0.8121^{+0.0082}_{-0.012}$	$0.8123^{+0.0087}_{-0.011}$	$0.810 \pm 0.011$	$0.810 \pm 0.011$	$0.8092^{+0.0089}_{-0.010}$
$\Omega_m$	$0.3070 \pm 0.0081$	$0.3009^{+0.0046}_{-0.0063}$	$0.3005^{+0.0043}_{-0.0057}$	$0.2984^{+0.0061}_{-0.0053}$	$0.2986 \pm 0.0066$	$0.2990^{+0.0046}_{-0.0062}$
$10^2 a_t$	$3.58^{+0.11}_{-0.41}$	$3.456^{+0.096}_{-0.28}$	$3.441^{+0.096}_{-0.27}$	$3.47^{+0.10}_{-0.29}$	$3.47^{+0.10}_{-0.30}$	$3.462^{+0.094}_{-0.29}$
$n$	1	2	3	4	6	> 3.05
Total $\chi^2$	3869.5714	3853.0243	3852.8177	3853.0654	3852.8015	3854.1713
$\Delta\chi^2$	13.843	-2.7041	-2.9107	-2.663	-2.9269	-1.55

TABLE VII: The mean  $\pm 1\sigma$ (best-fit) constraints on the cosmological parameters inferred from the *Planck* 2018 CMB data (including TTEETE + lensing), BAO, SNe, SH0ES and DES-Y1 data for  $\Lambda$ CDM and Canonical Emergent DE scenario with different values of  $n$  varying from 1 to 6.

#### A.4. Planck + Lensing + BAO + $H_0$ + DES-Y1 + HSC + KIDS

Constraints from Planck 2018 + Lensing + BAO + SN +  $H_0$  + DES + HSC + KIDS for  
Canonical Emergent DE

Parameter	$n = 1$	$n = 2$	$n = 3$	$n = 4$	$n = 6$
$H_0$	$67.61^{+0.46}_{-0.40}$	$69.01 \pm 0.68$	$69.16^{+0.42}_{-0.57}$	$69.16^{+0.39}_{-0.44}$	$68.99^{+0.49}_{-0.44}$
$\sigma_8$	$0.7933^{+0.0055}_{-0.0074}$	$0.8076^{+0.0055}_{-0.0069}$	$0.8088^{+0.0055}_{-0.0080}$	$0.8077^{+0.0058}_{-0.0069}$	$0.8083 \pm 0.0071$
$S_8$	$0.8016^{+0.0082}_{-0.011}$	$0.8041^{+0.0088}_{-0.0099}$	$0.804 \pm 0.011$	$0.803 \pm 0.010$	$0.8057^{+0.0079}_{-0.0097}$
$\Omega_m$	$0.3064^{+0.0046}_{-0.0064}$	$0.2975^{+0.0049}_{-0.0057}$	$0.2965 \pm 0.0078$	$0.2962 \pm 0.0049$	$0.2981^{+0.0044}_{-0.0057}$
$10^2 a_t$	$3.529^{+0.089}_{-0.36}$	$3.434^{+0.077}_{-0.26}$	$3.474^{+0.057}_{-0.30}$	$3.441^{+0.091}_{-0.27}$	$3.405^{+0.077}_{-0.23}$
Total $\chi^2$	3873.4982	3857.2683	3857.9786	3856.8311	3857.0445
$\Delta\chi^2$	13.6864	-2.5435	-1.8332	-2.9807	-2.7673

TABLE VIII: The mean  $\pm 1\sigma$  constraints on the cosmological parameters inferred from the *Planck* 2018 CMB data (including TTEETE + lensing), BAO, SNe, SH0ES, DES-Y1 and weak-lensing data for  $\Lambda$ CDM and Canonical Emergent DE scenario with different values of  $n$  varying from 1 to 6.

### A.5. Planck + Lensing + BAO + DES-Y1 + HSC + KIDS

Constraints from Planck 2018 + Lensing + BAO + SN + DES + KIDS + HSC for Canonical Emergent DE

Parameter	$n = 1$	$n = 2$	$n = 3$	$n = 4$	$n = 6$
$H_0$	$67.23^{+0.41}_{-0.32}$	$68.63^{+0.37}_{-0.33}$	$68.76^{+0.33}_{-0.39}$	$68.74 \pm 0.40$	$68.77 \pm 0.39$
$\sigma_8$	$0.7921 \pm 0.0078$	$0.8058 \pm 0.0069$	$0.8078 \pm 0.0075$	$0.8075^{+0.0054}_{-0.0062}$	$0.8074^{+0.0056}_{-0.0064}$
$S_8$	$0.8068^{+0.0079}_{-0.010}$	$0.8080^{+0.0084}_{-0.0097}$	$0.8087 \pm 0.0094$	$0.8086 \pm 0.0094$	$0.8080 \pm 0.0085$
$\Omega_m$	$0.3112^{+0.0040}_{-0.0059}$	$0.3017^{+0.0036}_{-0.0049}$	$0.3006^{+0.0045}_{-0.0038}$	$0.3008 \pm 0.0049$	$0.3004 \pm 0.0045$
$10^2 a_t$	$3.473^{+0.076}_{-0.31}$	$3.379^{+0.058}_{-0.21}$	$3.383^{+0.060}_{-0.22}$	$3.36^{+0.12}_{-0.20}$	$3.358^{+0.052}_{-0.19}$
Total $\chi^2$	3853.8996	3846.3778	3846.0869	3845.8107	3846.0881
$\Delta\chi^2$	7.8223	0.3005	0.0096	-0.2666	0.0108

TABLE IX: The mean  $\pm 1\sigma$  constraints on the cosmological parameters inferred from the *Planck* 2018 CMB data (including TTEETE + lensing), BAO, SNe, DES-Y1 and weak-lensing data for  $\Lambda$ CDM and Canonical Emergent DE scenario with different values of  $n$  varying from 1 to 6.

## Appendix B: Clustering Emergent Dark Energy

### B.1. Planck TTTEEE only

Constraints from Planck 2018 CMB for Clustering Emergent Dark Energy

Parameter	$n = 1$	$n = 2$	$n = 3$	$n = 4$	$n = 6$
$H_0$	$66.63 \pm 0.65$	$68.62 \pm 0.93$	$68.90^{+0.82}_{-0.73}$	$69.02^{+0.84}_{-0.74}$	$68.89^{+0.90}_{-0.72}$
$\sigma_8$	$0.8371^{+0.0080}_{-0.012}$	$0.8633^{+0.0092}_{-0.012}$	$0.8638^{+0.0089}_{-0.012}$	$0.8649^{+0.0080}_{-0.013}$	$0.8632^{+0.0086}_{-0.012}$
$S_8$	$0.863^{+0.016}_{-0.019}$	$0.864^{+0.018}_{-0.022}$	$0.861^{+0.016}_{-0.020}$	$0.859^{+0.017}_{-0.019}$	$0.860^{+0.016}_{-0.019}$
$\Omega_m$	$0.3189^{+0.0086}_{-0.0099}$	$0.3009^{+0.0095}_{-0.012}$	$0.2979^{+0.0087}_{-0.011}$	$0.2964^{+0.0090}_{-0.011}$	$0.2980^{+0.0087}_{-0.012}$
$10^2 a_t$	$3.335^{+0.051}_{-0.17}$	$3.274^{+0.029}_{-0.11}$	$3.289^{+0.052}_{-0.13}$	$3.283^{+0.032}_{-0.12}$	$3.268^{+0.039}_{-0.10}$
Total $\chi^2$	2764.9465	2766.3194	2766.6314	2766.6984	2766.6043
$\Delta\chi^2$	0.7765	2.1494	2.4614	2.5284	2.4343

TABLE X: The mean  $\pm 1\sigma$  constraints on the cosmological parameters inferred from the *Planck* 2018 CMB data (including TTEETE) for  $\Lambda$ CDM and Clustering Emergent DE scenario with different values of  $n$  varying from 1 to 6.

## B.2. Planck + Lensing + BAO + $H_0$

Constraints from Planck 2018 + Lensing + BAO + SN +  $H_0$  for Clustering Emergent Dark Energy

Parameter	$n = 1$	$n = 2$	$n = 3$	$n = 4$	$n = 6$
$H_0$	$67.34^{+0.69}_{-0.29}$	$68.51^{+0.70}_{-0.38}$	$68.76^{+0.63}_{-0.46}$	$68.74^{+0.71}_{-0.43}$	$68.65^{+0.41}_{-0.35}$
$\sigma_8$	$0.8365^{+0.0063}_{-0.012}$	$0.8551^{+0.0059}_{-0.0091}$	$0.8540^{+0.0048}_{-0.011}$	$0.8145^{+0.0068}_{-0.010}$	$.8581^{+0.0061}_{-0.0076}$
$S_8$	$0.8487^{+0.0093}_{-0.019}$	$0.8578^{+0.0087}_{-0.016}$	$0.8531^{+0.0083}_{-0.017}$	$0.814^{+0.011}_{-0.017}$	$0.8591^{+0.0089}_{-0.010}$
$\Omega_m$	$0.3088^{+0.0039}_{-0.0095}$	$0.3020^{+0.0045}_{-0.0090}$	$0.2995^{+0.0055}_{-0.0079}$	$0.2999^{+0.0049}_{-0.0089}$	$0.3007^{+0.0046}_{-0.0057}$
$10^2 a_t$	$3.375^{+0.049}_{-0.21}$	$3.257^{+0.015}_{-0.094}$	$3.275^{+0.014}_{-0.11}$	$3.284^{+0.031}_{-0.12}$	$3.244^{+0.022}_{-0.080}$
Total $\chi^2$	3860.9091	3853.7403	3852.5179	3855.1856	3857.67
$\Delta\chi^2$	6.8811	-0.2877	-1.5101	1.1576	3.642

TABLE XI: The mean  $\pm 1\sigma$  constraints on the cosmological parameters inferred from the *Planck* 2018 CMB data (including TTEETE + lensing), BAO, SNe and SH0ES for  $\Lambda$ CDM and Clustering Emergent DE scenario with different values of  $n$  varying from 1 to 6.

### B.3. Planck + Lensing + BAO + $H_0$ + DES-Y1

Constraints from Planck 2018 + Lensing + BAO + SN +  $H_0$  + DES

Parameter	$n = 1$	$n = 2$	$n = 3$	$n = 4$	$n = 6$	$n$ open
$H_0$	$67.61^{+0.60}_{-0.29}$	$69.00 \pm 0.51$	$68.88^{+0.48}_{-0.36}$	$68.96^{+0.43}_{-0.27}$	$69.04^{+0.52}_{-0.42}$	$68.93^{+0.50}_{-0.30}$
$\sigma_8$	$0.8286^{+0.0061}_{-0.0088}$	$0.8505^{+0.0057}_{-0.0083}$	$0.8463^{+0.0058}_{-0.0072}$	$0.8527 \pm 0.0075$	$0.8534^{+0.0048}_{-0.0075}$	$0.830^{+0.019}_{-0.014}$
$S_8$	$0.8355^{+0.0082}_{-0.014}$	$0.844 \pm 0.023$	$0.8429^{+0.0078}_{-0.011}$	$0.8478^{+0.0072}_{-0.011}$	$0.8471^{+0.0087}_{-0.011}$	$0.825 \pm 0.027$
$\Omega_m$	$0.3051^{+0.0035}_{-0.0082}$	$0.2956 \pm 0.0060$	$0.2976^{+0.0043}_{-0.0061}$	$0.2966^{+0.0030}_{-0.0056}$	$0.2957^{+0.0049}_{-0.0066}$	$0.2967^{+0.0037}_{-0.0058}$
$10^2 a_t$	$3.301^{+0.035}_{-0.14}$	$3.228^{+0.011}_{-0.065}$	$3.220^{+0.011}_{-0.058}$	$3.218^{+0.012}_{-0.056}$	$3.221^{+0.011}_{-0.060}$	$3.244^{+0.020}_{-0.081}$
$n$	1	2	3	4	6	$3.35^{+0.78}_{-0.011}$
Total $\chi^2$	3865.0585	3860.6482	3859.5398	3861.9733	3863.1704	3855.541
$\Delta\chi^2$	9.3301	4.9198	3.8114	6.2449	7.442	0.1874

TABLE XII: The mean  $\pm 1\sigma$  constraints on the cosmological parameters inferred from the *Planck* 2018 CMB data (including TTEETE + lensing), BAO, SNe, SH0ES and DES-Y1 for  $\Lambda$ CDM and Clustering Emergent DE scenario with different values of  $n$  varying from 1 to 6.

### B.4. Planck + Lensing + BAO + $H_0$ + DES-Y1 + HSC + KIDS

Constraints from Planck 2018 + Lensing + BAO + SN +  $H_0$  + DES + KIDS + HSC

Parameter	$n = 1$	$n = 2$	$n = 3$	$n = 4$	$n = 6$
$H_0$	$67.61^{+0.65}_{-0.43}$	$68.99^{+0.56}_{-0.27}$	$68.98^{+0.66}_{-0.38}$	$69.07^{+0.43}_{-0.39}$	$69.41^{+0.38}_{-0.56}$
$\sigma_8$	$0.8242^{+0.0052}_{-0.0083}$	$0.844 \pm 0.019$	$0.8418 \pm 0.0088$	$0.8092^{+0.0056}_{-0.0083}$	$0.8496^{+0.0054}_{-0.0071}$
$S_8$	$0.8307^{+0.0086}_{-0.015}$	$0.8376^{+0.0070}_{-0.011}$	$0.8364^{+0.0087}_{-0.012}$	$0.8030^{+0.0084}_{-0.011}$	$0.837 \pm 0.033$
$\Omega_m$	$0.3049^{+0.0053}_{-0.0089}$	$0.2956^{+0.0031}_{-0.0070}$	$0.2962^{+0.0045}_{-0.0080}$	$0.2954^{+0.0045}_{-0.0054}$	$0.2909^{+0.0067}_{-0.0046}$
$10^2 a_t$	$3.260^{+0.018}_{-0.098}$	$3.210^{+0.011}_{-0.049}$	$3.2105^{+0.0096}_{-0.049}$	$3.254^{+0.017}_{-0.091}$	$3.2151^{+0.0054}_{-0.053}$
Total $\chi^2$	3871.3678	3869.4694	3867.4459	3859.2281	3871.5003
$\Delta\chi^2$	11.556	9.6576	7.6341	-0.5837	11.6885

TABLE XIII: The mean  $\pm 1\sigma$  constraints on the cosmological parameters inferred from the *Planck* 2018 CMB data (including TTEETE + lensing), BAO, SNe, SH0ES, DES-Y1 and weak-lensing data for  $\Lambda$ CDM and Clustering Emergent DE scenario with different values of  $n$  varying from 1 to 6.

### B.5. Planck + Lensing + BAO + DES-Y1 + HSC + KIDS

Constraints from Planck 2018 + Lensing + BAO + SN +  $H_0$  + DES

Parameter	$n = 1$	$n = 2$	$n = 3$	$n = 4$	$n = 6$
$H_0$	$67.51^{+0.41}_{-0.33}$	$68.87^{+0.44}_{-0.31}$	$68.97 \pm 0.44$	$68.82 \pm 0.37$	$68.90^{+0.46}_{-0.37}$
$\sigma_8$	$0.8234^{+0.0059}_{-0.0068}$	$0.8455^{+0.0057}_{-0.010}$	$0.8422^{+0.0052}_{-0.0070}$	$0.8081^{+0.0060}_{-0.0077}$	$0.8482 \pm 0.0090$
$S_8$	$0.8317^{+0.0074}_{-0.010}$	$0.8413^{+0.0058}_{-0.013}$	$0.8369^{+0.0084}_{-0.0096}$	$0.8059^{+0.0080}_{-0.0098}$	$0.8443^{+0.0074}_{-0.011}$
$\Omega_m$	$0.3061^{+0.0041}_{-0.0057}$	$0.2970^{+0.0038}_{-0.0058}$	$0.2963^{+0.0044}_{-0.0051}$	$0.2984^{+0.0040}_{-0.0048}$	$0.2973^{+0.0043}_{-0.0059}$
$10^2 a_t$	$3.253^{+0.021}_{-0.091}$	$3.2117^{+0.0082}_{-0.049}$	$3.2071^{+0.0099}_{-0.046}$	$3.241^{+0.030}_{-0.078}$	$3.2060^{+0.0072}_{-0.044}$
Total $\chi^2$	3854.213	3859.4984	3857.8257	3848.0467	3861.4739
$\Delta\chi^2$	8.1357	13.4211	11.7484	1.9694	15.3966

TABLE XIV: The mean  $\pm 1\sigma$  constraints on the cosmological parameters inferred from the *Planck* 2018 CMB data (including TTEETE + lensing), BAO, SNe, DES-Y1 and weak-lensing data for  $\Lambda$ CDM and Clustering Emergent DE scenario with different values of  $n$  varying from 1 to 6.

## Appendix C: Non canonical Emergent Dark Energy

### C.1. Planck TTTEEE only

Constraints from Planck 2018

Parameter	$n = 1$	$n = 2$	$n = 3$	$n = 4$	$n = 6$
$H_0$	$66.18 \pm 0.62$	$68.30 \pm 0.70$	$68.47^{+0.66}_{-0.74}$	$68.48 \pm 0.74$	$68.47 \pm 0.77$
$\sigma_8$	$0.7997^{+0.0077}_{-0.0090}$	$0.8132^{+0.0078}_{-0.0091}$	$0.8147^{+0.0075}_{-0.0098}$	$0.8146^{+0.0077}_{-0.0097}$	$0.8143^{+0.0079}_{-0.0092}$
$S_8$	$0.835 \pm 0.017$	$0.822 \pm 0.017$	$0.821 \pm 0.017$	$0.821 \pm 0.017$	$0.821 \pm 0.017$
$\Omega_m$	$0.3268 \pm 0.0091$	$0.3067 \pm 0.0089$	$0.3050 \pm 0.0091$	$0.3050 \pm 0.0092$	$0.3051 \pm 0.0094$
$10^2 a_t$	$3.414^{+0.066}_{-0.25}$	$3.375^{+0.056}_{-0.21}$	$3.372^{+0.053}_{-0.21}$	$3.372^{+0.058}_{-0.21}$	$3.372^{+0.054}_{-0.21}$
$c_s^2$	$0.64^{+0.29}_{-0.16}$	$0.66^{+0.27}_{-0.16}$	$0.65 \pm 0.21$	$0.65^{+0.28}_{-0.16}$	$0.66^{+0.28}_{-0.15}$
Total $\chi^2$	2765.6229	2766.0841	2765.7061	2765.8519	2765.4524
$\Delta\chi^2$	1.4529	1.9141	1.5361	1.6819	1.2824

TABLE XV: The mean  $\pm 1\sigma$  constraints on the cosmological parameters inferred from the *Planck* 2018 CMB data (including TTEETE ) data for  $\Lambda$ CDM and Non-canonical Emergent DE scenario with different values of  $n$  varying from 1 to 6.

### C.2. Planck 2018 + Lensing + BAO + SN + $H_0$

Constraints from Planck 2018 + Lensing + BAO + SN +  $H_0$

Parameter	$n = 1$	$n = 2$	$n = 3$	$n = 4$	$n = 6$
$H_0$	$67.52 \pm 0.36$	$68.72^{+0.55}_{-0.33}$	$68.83^{+0.44}_{-0.50}$	$68.79 \pm 0.39$	$68.89 \pm 0.53'$
$\sigma_8$	$0.8014^{+0.0069}_{-0.0088}$	$0.8154^{+0.0067}_{-0.0086}$	$0.8150^{+0.0065}_{-0.0078}$	$0.8247^{+0.0064}_{-0.0076}$	$0.8155^{+0.0064}_{-0.0080}$
$S_8$	$0.8121^{+0.0096}_{-0.011}$	$0.8174^{+0.0086}_{-0.014}$	$0.816 \pm 0.011$	$0.826 \pm 0.013$	$0.8156^{+0.0089}_{-0.011}$
$\Omega_m$	$0.3081 \pm 0.0048$	$0.3015^{+0.0038}_{-0.0067}$	$0.3007 \pm 0.0058$	$0.3010 \pm 0.0045$	$0.3001^{+0.0044}_{-0.0055}$
$10^2 a_t$	$3.502^{+0.097}_{-0.34}$	$3.408^{+0.080}_{-0.24}$	$3.417^{+0.077}_{-0.25}$	$3.405^{+0.083}_{-0.23}$	$3.425^{+0.081}_{-0.26}$
$c_s^2$	$< 0.665$	$0.61^{+0.28}_{-0.20}$	$0.66^{+0.23}_{-0.19}$	$0.61^{+0.19}_{-0.25}$	$0.65^{+0.27}_{-0.17}$
Total $\chi^2$	3860.7531	3852.0743	3851.7264	3851.8387	3851.6283
$\Delta\chi^2$	6.7251	-1.9537	-2.3016	-2.1893	-2.3997

TABLE XVI: The mean  $\pm 1\sigma$  constraints on the cosmological parameters inferred from the *Planck* 2018 CMB data (including TTEETE + lensing), BAO, SNe, SH0ES data for  $\Lambda$ CDM and non-canonical Emergent DE scenario with different values of  $n$  varying from 1 to 6.

### C.3. Planck + Lensing + BAO + $H_0$ + DES-Y1

Constraints from Planck 2018 + Lensing + BAO + SN +  $H_0$  + DES

Parameter	$n = 1$	$n = 2$	$n = 3$	$n = 4$	$n = 6$	$n$ open
$H_0$	$67.65^{+0.29}_{-0.43}$	$68.94^{+0.37}_{-0.48}$	$68.93^{+0.44}_{-0.36}$	$69.14^{+0.41}_{-0.56}$	$69.02^{+0.38}_{-0.46}$	$68.96 \pm 0.40$
$\sigma_8$	$0.7994^{+0.0061}_{-0.0096}$	$0.8125^{+0.0063}_{-0.0082}$	$0.8129^{+0.0063}_{-0.0085}$	$0.8126^{+0.0061}_{-0.0077}$	$0.8134^{+0.0065}_{-0.0079}$	$0.8125^{+0.0059}_{-0.0079}$
$S_8$	$0.8078^{+0.0098}_{-0.011}$	$0.811 \pm 0.011$	$0.8119^{+0.0098}_{-0.011}$	$0.8086^{+0.0089}_{-0.010}$	$0.8112^{+0.0087}_{-0.011}$	$0.8108^{+0.0084}_{-0.010}$
$\Omega_m$	$0.3064^{+0.0051}_{-0.0041}$	$0.2988^{+0.0052}_{-0.0046}$	$0.2992^{+0.0042}_{-0.0052}$	$0.2971^{+0.0059}_{-0.0052}$	$0.2984 \pm 0.0056$	$0.2988 \pm 0.0046$
$10^2 a_t$	$3.510^{+0.088}_{-0.35}$	$3.415^{+0.064}_{-0.25}$	$3.392^{+0.074}_{-0.23}$	$3.447^{+0.092}_{-0.27}$	$3.407^{+0.070}_{-0.24}$	$3.400^{+0.069}_{-0.23}$
$c_s^2$	$0.58 \pm 0.23$	$0.65^{+0.30}_{-0.14}$	$0.65^{+0.28}_{-0.16}$	$0.69^{+0.20}_{-0.18}$	$0.64^{+0.32}_{-0.14}$	$0.66^{+0.27}_{-0.15}$
$n$	1	2	3	4	6	$> 3.07$
Total $\chi^2$	3868.9616	3853.8864	3853.4742	3853.0872	3853.4632	3852.9647
$\Delta\chi^2$	13.2332	-1.842	-2.2542	-2.6412	-2.2652	-2.7637

TABLE XVII: The mean  $\pm 1\sigma$  constraints on the cosmological parameters inferred from the *Planck* 2018 CMB data (including TTEETE + lensing), BAO, SNe, SH0ES and DES-Y1 data for  $\Lambda$ CDM and non-canonical Emergent DE scenario with different values of  $n$  varying from 1 to 6.

### C.4. Planck + Lensing + BAO + $H_0$ + DES-Y1 + HSC + KIDS

Constraints from Planck 2018 + Lensing + BAO + SN +  $H_0$  + DES + KIDS + HSC

Parameter	$n = 1$	$n = 2$	$n = 3$	$n = 4$	$n = 6$
$H_0$	$67.66^{+0.48}_{-0.36}$	$69.03 \pm 0.70$	$69.20^{+0.42}_{-0.54}$	$69.12^{+0.40}_{-0.47}$	$69.24^{+0.27}_{-0.48}$
$\sigma_8$	$0.7957^{+0.0058}_{-0.0081}$	$0.8099^{+0.0049}_{-0.0085}$	$0.8126^{+0.0045}_{-0.011}$	$0.8102^{+0.0053}_{-0.0082}$	$0.8103^{+0.0055}_{-0.0083}$
$S_8$	$0.8037^{+0.0076}_{-0.012}$	$0.8068^{+0.0081}_{-0.010}$	$0.8074^{+0.0072}_{-0.013}$	$0.8060^{+0.0080}_{-0.011}$	$0.804 \pm 0.010$
$\Omega_m$	$0.3061^{+0.0043}_{-0.0062}$	$0.2977 \pm 0.0074$	$0.2962 \pm 0.0060$	$0.2969 \pm 0.0063$	$0.2957^{+0.0053}_{-0.0035}$
$10^2 a_t$	$3.486^{+0.071}_{-0.32}$	$3.422^{+0.066}_{-0.25}$	$3.454^{+0.072}_{-0.29}$	$3.407^{+0.052}_{-0.24}$	$3.424^{+0.053}_{-0.26}$
$c_s^2$	$0.59^{+0.20}_{-0.23}$	$0.69^{+0.23}_{-0.15}$	$> 0.592$	$0.681^{+0.31}_{-0.089}$	$0.69^{+0.29}_{-0.10}$
Total $\chi^2$	3872.2972	3857.2175	3857.2294	3856.8636	3856.7384
$\Delta\chi^2$	12.4852	-2.5943	-2.5824	-2.9482	-3.0734

TABLE XVIII: The mean  $\pm 1\sigma$  constraints on the cosmological parameters inferred from the *Planck* 2018 CMB data (including TTEETE + lensing), BAO, SNe, SH0ES, DES-Y1 and weak-lensing data for  $\Lambda$ CDM and non-canonical Emergent DE scenario with different values of  $n$  varying from 1 to 6.

### C.5. Planck + Lensing + BAO + DES-Y1 + HSC + KIDS

Constraints from Planck 2018 + Lensing + BAO + SN + DES + KIDS + HSC

Parameter	$n = 1$	$n = 2$	$n = 3$	$n = 4$	$n = 6$
$H_0$	$67.35 \pm 0.33$	$68.69 \pm 0.39$	$68.77 \pm 0.38$	$68.81^{+0.34}_{-0.40}$	$68.79 \pm 0.40$
$\sigma_8$	$0.7947^{+0.0055}_{-0.0071}$	$0.8083^{+0.0054}_{-0.0066}$	$0.8091^{+0.0058}_{-0.0070}$		$0.8091^{+0.0054}_{-0.0068}$
$S_8$	$0.8076^{+0.0082}_{-0.0093}$	$0.8100^{+0.0080}_{-0.0090}$	$0.8100^{+0.0079}_{-0.0094}$	$0.8111^{+0.0082}_{-0.011}$	$0.8098^{+0.0082}_{-0.0093}$
$\Omega_m$	$0.3099 \pm 0.0044$	$0.3013 \pm 0.0046$	$0.3007 \pm 0.0045$	$0.3004 \pm 0.0047$	$0.3006 \pm 0.0047$
$10^2 a_t$	$3.419^{+0.068}_{-0.25}$	$3.357^{+0.057}_{-0.19}$	$3.342^{+0.065}_{-0.18}$	$3.350^{+0.047}_{-0.18}$	$3.333^{+0.043}_{-0.17}$
$c_s^2$	$0.62^{+0.20}_{-0.23}$	$> 0.585$	$0.68^{+0.25}_{-0.14}$	$> 0.582$	$> 0.595$
Total $\chi^2$	3853.5801	3845.4901	3845.5449	3845.2508	3845.3574
$\Delta\chi^2$	7.5028	-0.5872	-0.5324	-0.8265	-0.7199

TABLE XIX: The mean  $\pm 1\sigma$  constraints on the cosmological parameters inferred from the *Planck* 2018 CMB data (including TTEETE + lensing), BAO, SNe, DES-Y1 and weak-lensing data for  $\Lambda$ CDM and non-canonical Emergent DE scenario with different values of  $n$  varying from 1 to 6.